Adaptation of Delayed Position Feedback to the Reduction of Sway of Container Cranes

Nader A. Nayfeh

Thesis submitted to the Faculty of the
Virginia Polytechnic Institute and State University
in partial fulfillment of the requirements for the degree of

Master of Science
in
Electrical Engineering

William T. Baumann, Co-chair
Ziyad N. Masoud, Co-chair
Daniel J. Stilwell

December 4, 2002
Blacksburg, Virginia

Keywords: Container cranes, delayed feedback control, gantry crane, sway reduction

Adaptation of Delayed Position Feedback to the Reduction of Sway of Container Cranes

Nader A. Nayfeh

(ABSTRACT)

Cranes are increasingly used in transportation and construction. Increasing demand and faster requirements necessitate better and more efficient controllers to guarantee fast turn-around time and to meet safety requirements. Container cranes are used extensively in ship-to-port and port-to-ship transfer operations.

In this work, we will extend the recently developed delayed position feedback controller to container cranes. In contrast with traditional work, which models a crane as a simple pendulum consisting of a hoisting cable and a lumped mass at its end, we have modeled the crane as a four-bar mechanism. The actual configuration of the hoisting mechanism is significantly different from a simple pendulum. It consists typically of a set of four hoisting cables attached to four different points on the trolley and to four points on a spreader bar. The spreader bar is used to lift the containers. Therefore, the dynamics of hoisting assemblies of large container cranes are different from that of a simple pendulum. We found that a controller which treats the system as a four-bar mechanism has an improved response.

We developed a controller to meet the following requirements: traverse an 80-ton payload 50 m in 21.5 s, including raising the payload 15 m at the beginning and lowering the payload 15 m at the end of motion, while reducing the sway to 50 mm within 5.0 s at the end of the transfer maneuver. The performance of the controller has been demonstrated theoretically using numerical simulation. Moreover, the performance of the controller has been demonstrated experimentally using a 1/10th scale model. For the 1/10th scale model, the requirements translate into: traverse an 80 kg payload 5 m in 6.8 s, including raising 1.5 m at the beginning and lowering 1.5 m at the end of motion, while reducing the sway to 5 mm in under 1.6 s. The experiments validated the controller.

Dedication

To my family.

Contents

List of Figures

Chapter 1

Introduction

Cranes are increasingly used in transportation and construction. An example crane is shown in Figure 1.1. The increasing demand for faster and higher requirements necessitates better and more efficient controllers to guarantee fast turn-around time and to meet safety requirements. Consequently, there has been a boom in the research on the modeling and control of cranes (Abdel-Rahman et al., 2002). Most of these controllers developed have been far from satisfactory. In computer simulations, with simplified models they produce satifactory performance. However, when applied to physical systems, models or actual cranes, they fail.

A crane consists of a hoisting mechanism that is attached to a support mechanism. Typically, the hoisting mechanism consists of one or more cables and a hooking mechanism. In container cranes Figure 1.1, the hoisting mechanism would be the four cables and the spreader bar attached to the payload. Typical support mechanisms are trolley-girders, trolley-jibs, or booms. The hoisting assembly is suspended from one or more points on the support mechanism. The support mechanism moves the suspension point or points around the crane work space. In Figure 1.1, an example support structure would be the girder that allows for a traversing motion. The hoisting mechanism lifts and lowers the payload to avoid obstacles in its path and deposits the payload at the target point.

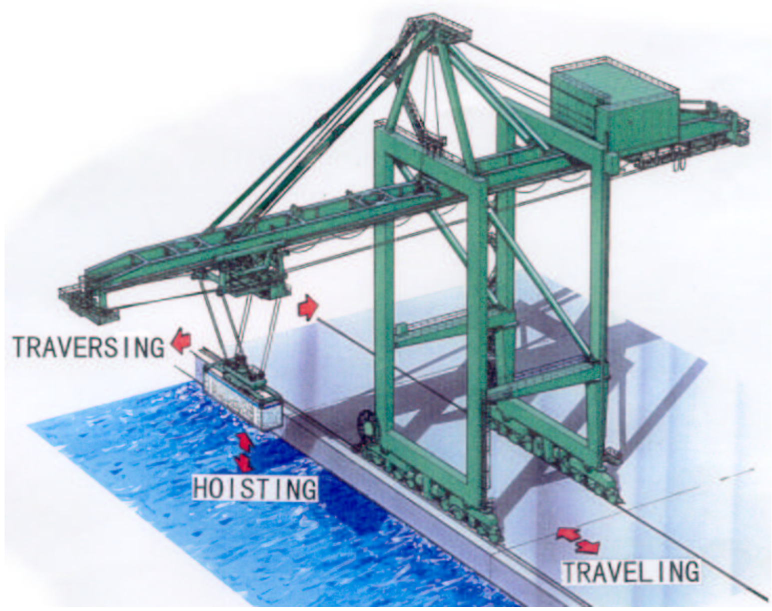

Figure 1.1: A typical container crane.

Cranes are classified by the degrees of freedom the support mechanism offers the suspension point. A “boom crane” has the suspension point fixed at the end of a boom. It has two degrees of freedom which consist of rotations around two orthogonal axes located at the base of the boom. A gantry crane is composed of a trolley moving on a girder along a single axis. In some gantry cranes, the girder is mounted on a second set of orthogonal railings, adding another degree of freedom in the horizontal plane. This configuration allows two translational degrees of freedom in the horizontal plane. A rotary crane has a suspension point moving along a girder, or jib, which is rotating in the horizontal plane about a fixed vertical axis. Thus, it has two degrees of freedom in the horizontal plane, translation and rotation.

Container cranes, as in Figure 1.1 are a subset of gantry cranes. Inertial forces on these cranes due to commanded trajectories or operator commands can cause the payload to have large sway angles, or pendulations. To avoid the pendulations, operators of the container cranes slow down operations so that the pendulations do not cause safety concerns and possible damage to the payload. However, slowing operations down increases the time that a ship is in port and at dock, thereby increasing the cost of loading and unloading operations.

The highly complicated hoisting mechanism used in container cranes results in complex system dynamics. External excitations, such as wind, can produce in-plane and out-of-plane pendulations as well as vertical oscillations of the payload. Even in the absence of external excitations, inertia forces due to the motion of the crane can induce significant payload pendulations. This problem is exacerbated by the fact that cranes are typically lightly damped, which means that any transient motion takes a long time to dampen out. Todd et al. (1997) reported that the damping in ship-mounted boom cranes is 0.1% to 0.5% of their critical damping. Patel et al. (1987) offered a higher estimate of 1% for the vertical motion and 5% for the lateral motions. Using numerical simulations Willemstein et al. (1986), van den Boom et al. (1987 and 1988), Patel et al. (1987), and Michelsen and Coppens (1988) demonstrated that the effect of stationary and transient dynamic forces produced by payload motions are large enough that they need to be accounted for in the design and operation of cranes. These findings emphasize the need to predict and control both the transient and stationary response of the payload.

One of the common recent strategies of controlling payload pendulations without including the operator in the control loop is "Input Shaping" (Abdel-Rahman et al., 2002). For a predefined endpoint of transport, the input shaping controller adjusts the length of the hoist cable and drives the suspension point of the payload along predefined (shaped) trajectories that avoid exciting payload pendulations. Parker et al. (1995) used input shaping techniques on a three-dimensional linear time-varying model of a rotary crane to optimize the commanded input signal so as to avoid exciting the payload pendulations in rest-to-rest maneuvers.

Alsop et al. (1965) presented a two-dimensional linear model of a gantry crane. They proposed an input shaping strategy in which the controller accelerates in steps of constant acceleration and then kills the acceleration when the load reaches a zero-pendulation angle. The same approach is used in the deceleration stage. Computer simulations were conducted using two constant acceleration/deceleration steps.

Jones and Petterson (1988) extended the work of Alsop et al. (1965) by using a nonlinear approximation of the pendulation period to generate an analytical expression for the duration of the coasting stage as a function of the amplitude and duration of the constant acceleration steps. They then used this analytical expression to generate a two-step acceleration profile. Numerical simulations using various acceleration profiles showed that this technique was able to reduce the residual pendulations to about 0.1° to 0.3°. However, it was not able to dampen out initial disturbances of the payload and external disturbances during the transfer maneuver. In fact, it could even amplify them. Furthermore, significant time losses were observed. Noakes et al. (1990) and Noakes and Jansen (1990, 1992) applied a one-step variation of this acceleration profile to an actual bidirectional crane by using a constant cable length and performing a U-shaped maneuver. Their test results matched those of the numerical simulations.

As a feed-forward strategy, residual pendulations due to unmodeled nonlinearities still exist. Feedback techniques are then used to dampen out these pendulations, adding more time to the transfer maneuver. Dadone and VanLandingham (2002) generated a better approximation of the cable-payload period using the method of multiple scales. Using numerical simulation, they compared the residual pendulations due to one-step input shaping strategies based on their nonlinear approximation, a simplified form of that approximation, and the linear approximation of the period. They discovered a significant enhancement, of as much as two orders of magnitude, in the performance of the nonlinear control strategies over the linear strategy. The enhanced performance with the nonlinear approximation was most pronounced for longer coasting distances and higher accelerations.

Optimal control techniques and input shaping techniques are limited by the fact that they are extremely sensitive to variations in the parameter values about the nominal values, and are extremely sensitive to changes in the initial conditions and external disturbances. They require “highly accurate values of the system parameters” to achieve a satisfactory system response (Zinober and Fuller, 1973; Virkkunen and Marttinen, 1988; Yoon et al., 1995). While a good design can minimize the controller's sensitivity to changes in the payload mass and shape, it is much harder to alleviate the controller's sensitivity to changes in the cable length. In fact, Singhose et al. (1997) showed that input shaping techniques are sensitive to the pendulation natural frequency. As a result, they suffer significant degradation in crane maneuvers that involve hoisting. Furthermore, input shaping and optimal control techniques require a predetermined endpoint of the transport maneuver. This makes them less practical because most crane operations are coordinated visually by the crane operator. Linear controllers and static feedback linearization control techniques have very poor performance and usually fail due to the highly nonlinear nature of the payload oscillations (d'Andrea-Novel and Levine, 1989).

Henry et al. (2001) and Masoud et al. (2002, 2002, 2002) developed a strategy by which cargo pendulations of a crane payload are significantly suppressed by forcing the suspension point of the payload hoisting cable to track inertial reference coordinates. The reference coordinates consist of a percentage of the delayed motion of the payload in the inertial horizontal plane relative to the suspension point superimposed on the operator commanded motion. For boom cranes, the payload pendulations in and out of the boom and tower plane are controlled by simply actuating the luff and slew angles of the boom. These degrees of freedom already exist in boom cranes, and therefore modification to the hardware of current cranes would be limited to the addition of a few sensors and electronics to execute the control algorithm. The control strategy is based on time-delayed position feedback of the payload cable angles. This control algorithm is superimposed transparently on the input of the crane operator, which eliminates any special training requirements for crane operators and furnishes smoother and faster transfer operations. The stability of the in-plane payload pendulations using the delayed position feedback controller was investigated by Henry et al. (2001) and was proven to be robust under significantly large base excitations and large initial disturbance conditions. The effectiveness of the control strategy has been demonstrated using numerical simulations of computer models of boom, rotary, and gantry cranes. Furthermore, the control strategy has been applied to, and tested on, experimental scaled models of a rotary crane operating in both the rotary and gantry modes of operation and a ship-mounted boom crane excited by the motion of a platform with three degrees of freedom, which correspond to the heave, pitch, and roll of a ship.

The objective of this work is to apply the delayed position feedback controller developed by Henry et al. (2001) to container cranes. The requirements for the full scale operation are to move an 80-ton payload a distance of 50 m in 21.5 s, including raising the payload 15 m at the beginning and lowering the payload 15 m at the end of motion, while reducing the sway at the end of motion to less than 50 mm within 5.0 s. The methodology to derive the controller is verified by numerical simulation of a full nonlinear computer model of the container crane and controller. The theoretical results are validated experimentally using a 1/10th scale model of a container crane.

A nonlinear mathematical model of a container crane was developed. Instead of the usual lumped-mass (spherical pendulum) or distributed-mass models, a four-bar mechanism formulation is used because the dynamics of the hoisting assembly of large container cranes are different from those of a simple pendulum. Then a simplified model was derived to determine the gain and delay for the controller. Using these parameters, we demonstrated the effectiveness of the controller numerically using the full nonlinear model of the container crane.

The controller was validated experimentally on a 1/10th scale model of a container crane at the IHI Yokohama plant. The requirements for operation were to move an 80 kg load 5.0 m in 6.8 s along with different hoisting trajectories. After 1.6 s of the end of motion, the payload sway needed to be reduced to under 5 mm. Significant match between the experimental results and numerical simulations was observed.

Chapter 2

Modeling

2.1 Introduction

In this chapter, we develop a full nonlinear model for container cranes by modeling the trolley, payload, and hoisting mechanism as a four-bar mechanism. Then, a simplified model is developed, which is used in determining the gain and time delay for the controller. Finally, the controller is designed using the simplified model.

2.2 Full Nonlinear Model

The equations of motion for the four-bar mechanism model of the container crane, Figure 2.1, can be derived using the Euler-Lagrange equations

$$\frac{d}{dt}\left[\frac{\partial \mathcal{L}}{\partial \dot{x}}\right] - \frac{\partial \mathcal{L}}{\partial x} = 0 \tag{2.1}$$

$$\frac{d}{dt}\left[\frac{\partial \mathcal{L}}{\partial \dot{y}}\right] - \frac{\partial \mathcal{L}}{\partial y} = 0 \tag{2.2}$$

$$\frac{d}{dt}\left[\frac{\partial \mathcal{L}}{\partial \dot{\theta}}\right] - \frac{\partial \mathcal{L}}{\partial \theta} = 0. \tag{2.3}$$

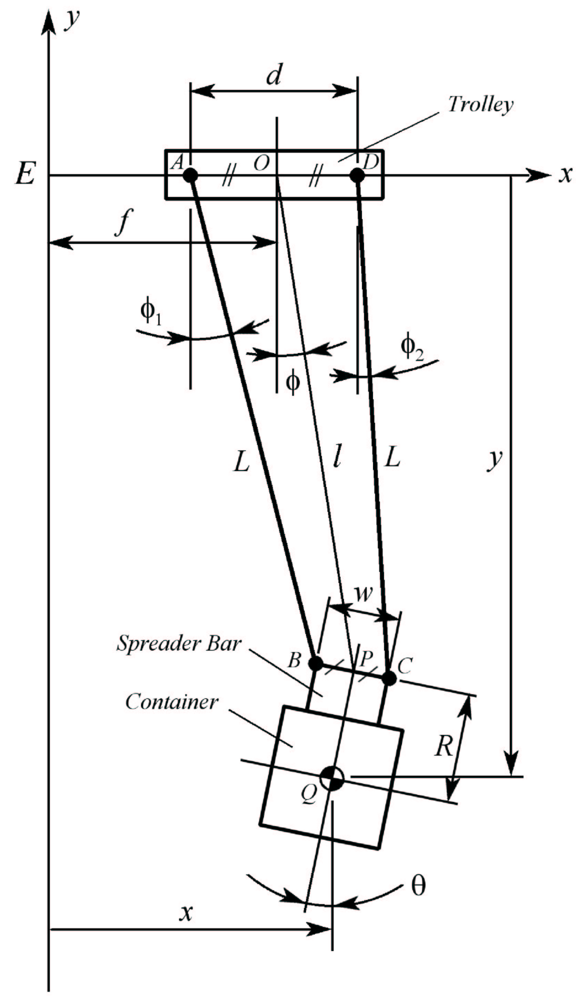

Figure 2.1: A schematic model of a container crane.

where $\mathcal{L}$ is the Lagrangian defined as

$$\mathcal{L} \equiv K - V \tag{2.4}$$

and K is the kinetic energy and V is the potential energy of the payload.

The kinetic energy is easily determined to be

$$K = \frac{1}{2}m(\dot{x}^2 + \dot{y}^2) + \frac{1}{2}J\dot{\theta}^2 \tag{2.5}$$

where m is the mass of the load and spreader bar and J is the mass moment of inertia of the combined load and spreader bar about their center of gravity, point Q. The potential energy V is also determined to be

$$V = mgy \tag{2.6}$$

Substituting (2.5) and (2.6) into (2.4) produces

$$\mathcal{L} = \frac{1}{2}m(\dot{x}^2 + \dot{y}^2) + \frac{1}{2}J\dot{\theta}^2 - mgy \tag{2.7}$$

Since the model in Figure 2.1 is a four-bar mechanism, constraints on the system must be developed. The goal is to find the vectors **AB** and **DC** using the (x,y,θ) coordinates, where θ is the rotation angle of the load. First, a vector **EQ** is defined from the origin E to point Q as

$$\mathbf{EQ} = (x, -y) \tag{2.8}$$

Then, a vector **EA** is defined from the origin E to point A as

$$\mathbf{EA} = (f(t) - \frac{1}{2}d, 0), \tag{2.9}$$

where $f(t)$ is the driving function of the trolley and d is the cable spacing at the trolley.

From geometry the vectors **QP** and **PB** are defined as

$$\mathbf{QP} = (R\sin\theta, R\cos\theta) \tag{2.10}$$

$$\mathbf{PB} = (-\frac{1}{2}w\cos\theta, \frac{1}{2}w\sin\theta) \tag{2.11}$$

Then, the vector **QB** becomes

$$\mathbf{QB} = \mathbf{QP} + \mathbf{PB} \tag{2.12}$$

$$= (R\sin\theta - \frac{1}{2}w\cos\theta, R\cos\theta + \frac{1}{2}w\sin\theta) \tag{2.13}$$

Summing the vectors **QB** and **EQ** produces

$$\mathbf{EB} = (x + R\sin\theta - \frac{1}{2}w\cos\theta, -y + R\cos\theta + \frac{1}{2}w\sin\theta) \tag{2.14}$$

Then, the vector **AB** can be expressed as

$$\begin{aligned}\mathbf{AB} &= \mathbf{EB} - \mathbf{EA} \qquad (2.15)\\ &= (x + R\sin\theta - \frac{1}{2}w\cos\theta - f(t) + \frac{1}{2}d, -y + R\cos\theta + \frac{1}{2}w\sin\theta) \qquad (2.16)\end{aligned}$$

Similary, the vector **DC** can be derived as

$$\mathbf{DC} = (x + R\sin\theta + \frac{1}{2}w\cos\theta - f(t) - \frac{1}{2}d, -y + R\cos\theta - \frac{1}{2}w\sin\theta) \qquad (2.17)$$

Finally, the contraints are determined by using the Pythagareon Theorem as

$$(x + R\sin\theta - \frac{1}{2}w\cos\theta - f(t) + \frac{1}{2}d)^2 + (y - R\cos\theta - \frac{1}{2}w\sin\theta)^2 - L^2 = 0 \qquad (2.18)$$

$$(x + R\sin\theta + \frac{1}{2}w\cos\theta - f(t) - \frac{1}{2}d)^2 + (y - R\cos\theta + \frac{1}{2}w\sin\theta)^2 - L^2 = 0 \qquad (2.19)$$

where L is the length of the hoist cable.

Now, multiplying the constraints, (2.18) and (2.19), by the Lagrange multipliers, λ_1 and λ_2, respectively, and adding them to (2.7) gives the augmented Lagrangian

$$\begin{aligned}\mathcal{L}_a &= \frac{1}{2}m(\dot{x}^2 + \dot{y}^2) + \frac{1}{2}J\dot{\theta}^2 - mgy \qquad (2.20)\\ &+ \lambda_1\left[(x + R\sin\theta - \frac{1}{2}w\cos\theta - f(t) + \frac{1}{2}d)^2 + (y - R\cos\theta - \frac{1}{2}w\sin\theta)^2 - L(t)^2\right]\\ &+ \lambda_2\left[(x + R\sin\theta + \frac{1}{2}w\cos\theta - f(t) - \frac{1}{2}d)^2 + (y - R\cos\theta + \frac{1}{2}w\sin\theta)^2 - L(t)^2\right]\end{aligned}$$

Applying the Euler-Lagrange equations to (2.20) gives the following fully nonlinear equations of motion for the four-bar model of a container crane:

$$\begin{aligned}m\ddot{x} - (2\lambda_1(x + R\sin\theta - \frac{1}{2}w\cos\theta - f(t) + \frac{1}{2}d) \qquad (2.21)\\ +2\lambda_2(x + R\sin\theta + \frac{1}{2}w\cos\theta - f(t) - \frac{1}{2}d)) &= 0\end{aligned}$$

$$m\ddot{y} - (2\lambda_1(y - R\cos\theta - \frac{1}{2}w\sin\theta) + 2\lambda_2(y - R\cos\theta + \frac{1}{2}w\sin\theta)) + mg = 0 \qquad (2.22)$$

$$J\ddot{\theta} - 2\lambda_1\left[\left(R\cos\theta + \frac{1}{2}w\sin\theta\right)\left(x - \frac{1}{2}w\cos\theta - f(t) + R\sin\theta + \frac{1}{2}d\right)\right.$$

$$
\begin{aligned}
& + \left(R\sin\theta - \frac{1}{2}w\cos\theta\right)\left(y - R\cos\theta - \frac{1}{2}w\sin\theta\right)\Bigg] \\
-2\lambda_2 & \left[\left(R\cos\theta - \frac{1}{2}w\sin\theta\right)\left(x + \frac{1}{2}w\cos\theta - f(t) + R\sin\theta - \frac{1}{2}d\right)\right. \\
& \left. + \left(R\sin\theta - \frac{1}{2}w\cos\theta\right)\left(y - R\cos\theta - \frac{1}{2}w\sin\theta\right)\right] = 0
\end{aligned} \tag{2.23}
$$

Now, in order to solve the three equations of motion using the two contraint equations, we need to differentiate (2.18) and (2.19) twice in time. The differentiation provides us with two more differential equations. We differentiate (2.18) and (2.19) twice with respect to t and obtain

$$
\begin{aligned}
g_{11}\ddot{x} + g_{12}\ddot{y} + g_{13}\ddot{\theta} &+ 2\dot{x}^2 + 2\dot{y}^2 + g_{14}\dot{\theta}^2 + g_{15}\dot{\theta}\dot{x} \\
&+ g_{16}\dot{\theta}\dot{y} + g_{17}\dot{\theta}\dot{f} + g_{18}\ddot{f} + 4\dot{f}\dot{x} - 2\dot{f}^2 = 0
\end{aligned} \tag{2.24}
$$

and

$$
\begin{aligned}
g_{21}\ddot{x} + g_{22}\ddot{y} + g_{23}\ddot{\theta} &+ 2\dot{x}^2 + 2\dot{y}^2 + g_{24}\dot{\theta}^2 + g_{25}\dot{\theta}\dot{x} \\
&+ g_{26}\dot{\theta}\dot{y} + g_{27}\dot{\theta}\dot{f} + g_{28}\ddot{f} + 4\dot{f}\dot{x} - 2\dot{f}^2 = 0
\end{aligned} \tag{2.25}
$$

where

$$g_{m1} = -(-1)^m d + (-1)^m w\cos\theta - 2f + 2R\sin\theta + 2x \tag{2.26}$$

$$g_{m2} = -2R\cos\theta + (-1)^m w\sin\theta + 2y \tag{2.27}$$

$$
\begin{aligned}
g_{m3} &= -(-1)^m dR\cos\theta - 2Rf\cos\theta + \frac{1}{2}dw\sin\theta + (-1)^m wf\sin\theta \\
&+ 2Rx\cos\theta - (-1)^m wx\sin\theta + (-1)^m wy\cos\theta + 2Ry\sin\theta
\end{aligned} \tag{2.28}
$$

$$
\begin{aligned}
g_{m4} &= \frac{1}{2}dw\cos\theta + (-1)^m wf\cos\theta + (-1)^m dR\sin\theta + 2Rf\sin\theta \\
&- (-1)^m wx\cos\theta - 2Rx\sin\theta + 2Ry\cos\theta - (-1)^m wy\sin\theta
\end{aligned} \tag{2.29}
$$

$$g_{m5} = 4R\cos\theta - (-1)^m 2w\sin\theta \tag{2.30}$$

$$g_{m6} = (-1)^m 2w\cos\theta + 4R\sin\theta \tag{2.31}$$

$$g_{m7} = 4R\cos\theta - (-1)^m 2w\sin\theta \tag{2.32}$$

$$g_{m8} = (-1)^m d - (-1)^m w\cos\theta + 2f - 2R\sin\theta - 2x \tag{2.33}$$

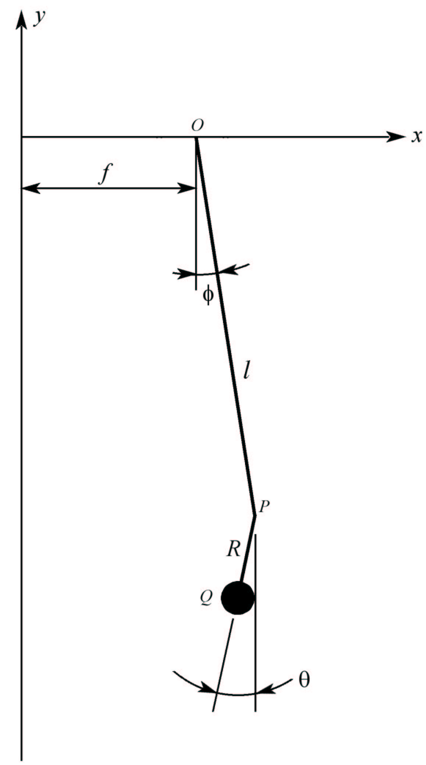

Figure 2.2: A simplified schematic model of a container crane.

Now, we have three equations of motion and two constraint equations. We solve them numerically, for x, y, θ, λ_1, and λ_2 , using a combination of Simulink and Matlab.

2.3 Simplified Model

The container crane model, Figure 2.1, can be simplified as a double pendulum system with two fixed-length links, and a kinematic constraint relating the angles ϕ and θ, as shown in Figure 2.2. To this end, we let $\mathbf{OP} = l$. Then, the closing constraints of the loop $AOPB$ in

Figure 2.1 can be written as

$$l\sin\phi - \frac{1}{2}w\cos\theta + \frac{1}{2}d = L\sin\phi_1 \tag{2.34}$$

$$l\cos\phi - \frac{1}{2}w\sin\theta = L\cos\phi_1 \tag{2.35}$$

Similarly, the closing constraints of the loop $ODCP$ can be written as

$$l\sin\phi + \frac{1}{2}w\cos\theta - \frac{1}{2}d = L\sin\phi_2 \tag{2.36}$$

$$l\cos\phi + \frac{1}{2}w\sin\theta = L\cos\phi_2 \tag{2.37}$$

Squaring and adding (2.34) and (2.35) yields

$$\left(l\cos\phi - \frac{1}{2}w\sin\theta\right)^2 + \left(l\sin\phi - \frac{1}{2}w\cos\theta + \frac{1}{2}d\right)^2 = L^2 \tag{2.38}$$

and squaring and adding (2.36) and (2.37) yields

$$\left(l\cos\phi + \frac{1}{2}w\sin\theta\right)^2 + \left(l\sin\phi + \frac{1}{2}w\cos\theta - \frac{1}{2}d\right)^2 = L^2 \tag{2.39}$$

Eliminating L^2 from (2.39) and (2.38) and manipulating the result, we obtain the following relation between ϕ and θ:

$$d\sin\phi = w\sin(\theta+\phi) \tag{2.40}$$

which for small oscillations reduces to

$$\theta = \frac{d-w}{w}\phi = a\phi \tag{2.41}$$

where $a = \frac{d-w}{w}$. Using (2.40) to simplify (2.39), we obtain

$$l^2 = L^2 - \frac{1}{4}\left(d^2 + w^2 - 2dw\cos\theta\right) \tag{2.42}$$

which for small oscillations reduces to

$$l^2 = L^2 - \frac{1}{4}(d-w)^2 \tag{2.43}$$

Next, we write the potential and kinetic energies of the system. To this end, we note that the coordinates of Q are

$$x = f(t) + l\sin\phi - R\sin\theta \tag{2.44}$$

$$y = -l\cos\phi - R\cos\theta \tag{2.45}$$

Then, differentiating (2.44) and (2.45) once with respect to time yields the velocity components

$$\dot{x} = \dot{f} + \dot{\phi}l\cos\phi - R\dot{\theta}\cos\theta \tag{2.46}$$

$$\dot{y} = l\dot{\phi}\sin\phi + R\dot{\theta}\sin\theta \tag{2.47}$$

For small oscillations, (2.46) and (2.47) become

$$\dot{x} = \dot{f} + l\dot{\phi} - R\dot{\theta} \tag{2.48}$$

$$\dot{y} = 0 \tag{2.49}$$

Hence, for small oscillations,

$$\dot{v}^2 = \dot{x}^2 + \dot{y}^2 = \left(\dot{f} + L\dot{\phi} - R\dot{\theta}\right)^2 \tag{2.50}$$

where v is the velocity. Which upon using (2.41) becomes

$$\dot{v}^2 = \left[\dot{f} + (l - aR)\dot{\phi}\right]^2 \tag{2.51}$$

The kinetic energy is given by

$$K = \frac{1}{2}m\left[(l - aR)\dot{\phi} + \dot{f}\right]^2 \tag{2.52}$$

And the potential energy can be written as

$$V = mg\left[l - l\cos\phi + R - R\cos\theta\right] \tag{2.53}$$

which for small oscillations reduces to

$$V = \frac{1}{2}mg\left(l\phi^2 + R\theta^2\right) = \frac{1}{2}mg\left(l + a^2R\right)\phi^2 \tag{2.54}$$

Using (2.51) and (2.54), we write the Lagrangian of the motion as

$$\mathcal{L} = \frac{1}{2}m\left[(l-aR)\dot{\phi}+\dot{f}\right]^2 - \frac{1}{2}mg\left(l+a^2R\right)\phi^2 \tag{2.55}$$

Applying the Euler-Lagrange equation

$$\frac{d}{dt}\left[\frac{\partial\mathcal{L}}{\partial\dot{\phi}}\right] - \frac{\partial\mathcal{L}}{\partial\phi} = 0 \tag{2.56}$$

to (2.55), yields the equations of motion

$$\ddot{\phi} + \frac{\ddot{f}}{(l-aR)} + \frac{g(l+a^2R)}{(l-aR)^2}\phi = 0 \tag{2.57}$$

Adding a linear damping term for θ and for the trolley, $\frac{2\mu\dot{f}}{(l-aR)}$, to (2.57), we rewrite it as

$$\ddot{\phi} + \frac{\ddot{f}}{l-aR} + 2\mu\dot{\phi} + \frac{2\mu\dot{f}}{(l-aR)} + \frac{g(l+a^2R)}{(l-aR)^2}\phi = 0 \tag{2.58}$$

2.4 Controller Design

A delayed position feedback controller was developed earlier by Henry et al (2001). The controller has the following form:

$$f(t) = x_o(t) + G\sin\left[\phi(t-\tau)\right] \tag{2.59}$$

where $x_o(t)$ is the operator input, G is a gain, and τ is the time delay. Assuming that the operator input is a slow-varying term and substituting the general controller form, (2.59), into the simplified equation of motion of the system (2.58), we obtain the following linearized controlled equation describing the fast-varying dynamics:

$$\ddot{\phi}(t) + 2\mu\dot{\phi}(t) + \frac{G}{(l-aR)}\left[\ddot{\phi}(t-\tau)+2\mu\dot{\phi}(t-\tau)\right] + \frac{(l+a^2R)}{(l-aR)^2}g\phi(t) = 0 \tag{2.60}$$

where $l = \sqrt{L^2-(d-w)^2/4}$ and $2\mu\dot{\phi}(t)$ is an added damping term.

Choosing the controller gain $G = k(l-aR)$, we rewrite the controller equation as

$$f(t) = x_o(t) + k(l-aR)\sin\left[\phi(t-\tau)\right] \tag{2.61}$$

Substituting the chosen controller gain into the equation of motion, (2.60), we obtain

$$\ddot{\phi}(t) + 2\mu\dot{\phi}(t) + k\left[\ddot{\phi}(t-\tau) + 2\mu\dot{\phi}(t-\tau)\right] + \frac{(l+a^2R)}{(l-aR)^2}g\phi(t) = 0 \tag{2.62}$$

We note that the period of oscillation for this second order differential equation is

$$T = \frac{2\pi(l-aR)}{\sqrt{g(l+a^2R)}} \tag{2.63}$$

The linearized controlled equation of motion, (2.62), of the simplified system resembles the linearized controlled equation of motion of the simple pendulum in Henry et al. (2001) with a modified period of oscillation. Hence, the controller delay τ is now chosen based on this modified period T, given by (2.63). An appropriate combination of controller gain k and delay τ to produce the desired damping is selected from the damping chart in Figure 2.3, Henry et al. (2001). The darker the shading, the more damping is introduced by the controller.

A block diagram of the controller is given in Figure (2.4). The PID loop around the plant is used to track the commanded position of the trolley. We measure L and ϕ from the system. We then calculate l from (2.42) and T from (2.63). Next we determine k and τ. Then, the control signal is generated and combined with the operator command. Finally, it is fed back into the plant.

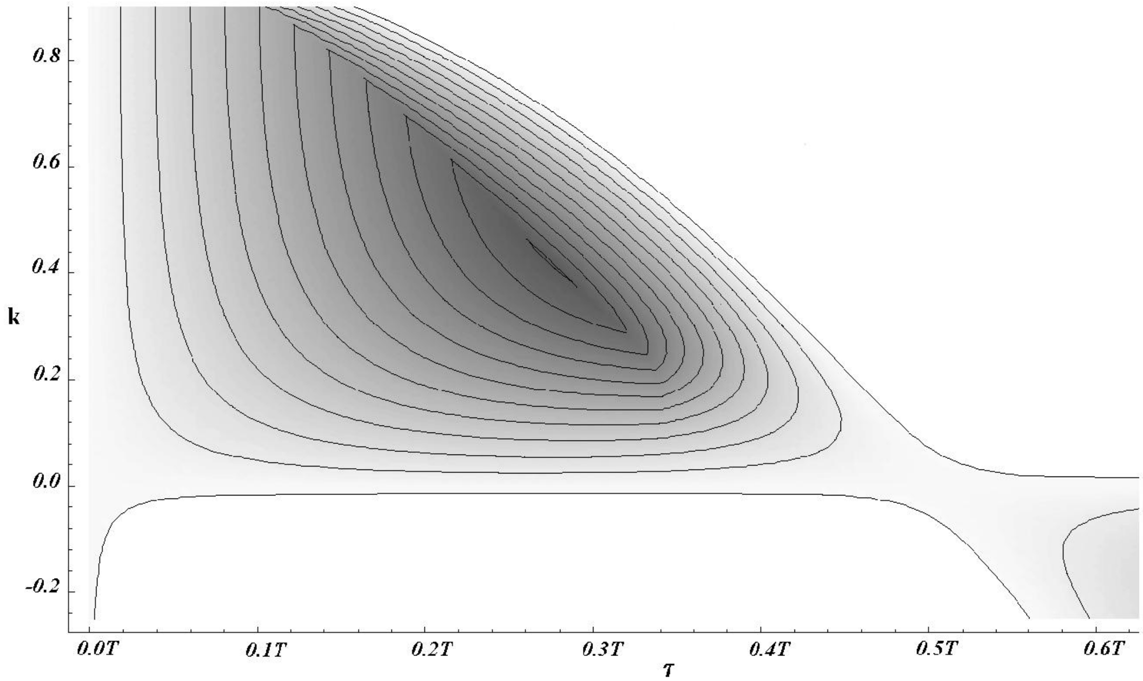

Figure 2.3: A contour plot of the damping as a function of the controller gain, k, and delay, τ. T is the natural period of the uncontrolled system. The darker areas correspond to higher damping.

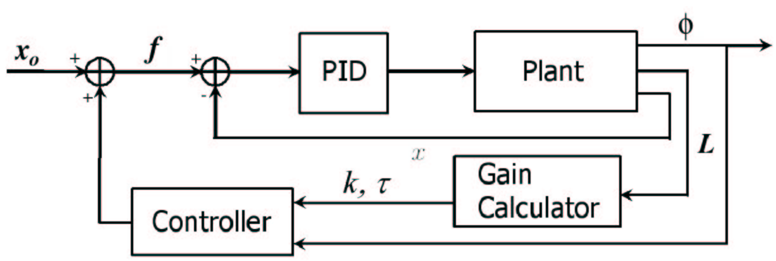

Figure 2.4: A block diagram of the controller and plant.

Chapter 3

Experimental Setup

3.1 The Control Unit

We built a custom control unit for implementing the delayed position feedback controller. The need for a self-contained portable unit with specific input and output requirements prompted this design. While the controller was designed to be stand-alone, an external interface was also desired. Hence, we chose a PC interface as the basis for the controller with a laptop computer networked to that PC as the external interface.

The basic premise for the portability of the controller is that it should be a small portable unit such as a small suitcase. Fortunately, there are several readily available commercial suitcases made out of materials, such as aluminum, that could be used as the basis for the self-contained control unit.

The actual controller can be implemented using a very simple microprocessor and a number of analog-to-digital converters (ADC's) and digital-to-analog converters (DAC's); however, since this control unit is intended for experimental work and the numbers and types of sensors may vary, we selected the control board based on the number and capability of its inputs and outputs. Basic requirements were a minimum of four quadrature encoder inputs with at least 4 analog inputs and 4 analog outputs. Also, the ADC's and DAC's had to have a sampling frequency of at least 100 Hz. Since the controller is PC based and because all of the newer computers have only PCI slots available, the control board also had to be PCI based. After an extensive search, the Aerotech U500 Ultra was deemed to be the best control board to meet the above requirements. The U500 Ultra has 8 quadrature encoder counters, 8 ADC's, and 8 DAC's. To interface with the U500 Ultra, the breakout boards that were required are the BB500 and two TBD50.

After deciding upon the controller and determining the size of the interface breakout boards, we established a rough estimate of the size of the self-contained unit. From this estimate, we purchased an aluminum suitcase made by Zero.

After receiving the various components of the controller, we took measurements of the suitcase and the layout for the electronics. Then, we designed the rest of the control unit. The material selected was all aluminum alloy 6061, because it is not only lightweight and easily machinable, but also sturdy.

Figure 3.1 shows a view of the aluminum suitcase and frame. The three wire assemblies that can be seen are external interfaces for a standard 15-pin video out, a PS/2 mouse, and a PS/2 keyboard. The black plug is a bridge for a RJ-45 ethernet cable connector.

Figure 3.2 shows a view of the suitcase with the mounting plate for the motherboard and breakout boards. Figure 3.3 shows a view of the control unit with the motherboard, BB500 breakout board, the two TBD50 breakout boards, video card, ethernet card, and power supply installed, but not yet wired. Figure 3.4 shows a view of the control unit with all of the hardware installed, including the hard-drive and U500 Ultra. Figure 3.5 shows the internal components of the control unit installed, including the wiring. Finally, Figure 3.6 shows how the finished control unit looks like, with the interface cables connected.

The interface between our control unit and the driving unit of the IHI experimental scaled model of the container crane was in fact very simple. Since our control unit was ready to go with coaxial and nine-pin connectors, it took only a day to acquire the cabling to the interface.

Figure 3.7 shows a basic connection diagram between the crane model and the control unit. Inputs to the control unit from the sensors were four optical quadrature encoders, which were connected to four nine-pin connectors. One encoder signal was from the trolley motor, one from the angle sensor, and two from the two hoist motors. Also, there were two analog inputs from the joystick controls: one for the traverse motion and the other for the hoist. Outputs from the control unit to the IHI unit were three analog outputs: one connection to the trolley motor and two to the hoist motors.

3.2 IHI's Crane Model

IHI provided us with access to a 1/10th scale model of a container crane at their Yokohama Research Facility. The model has a 5 m track, a 15 kg spreader bar, and a 65 kg load. The girder was approximately 4.5 m above the ground level. One DC brushless motor drives the traversing degree of freedom, while two DC brushless motors drive the hoisting degree of

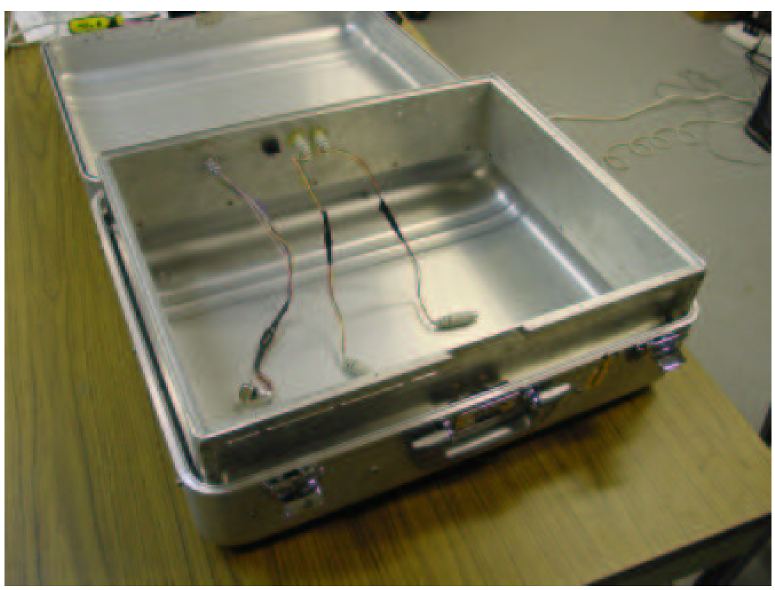

Figure 3.1: A view of the suitcase and frame.

Figure 3.2: A view of the suitcase, frame, and mounting plate.

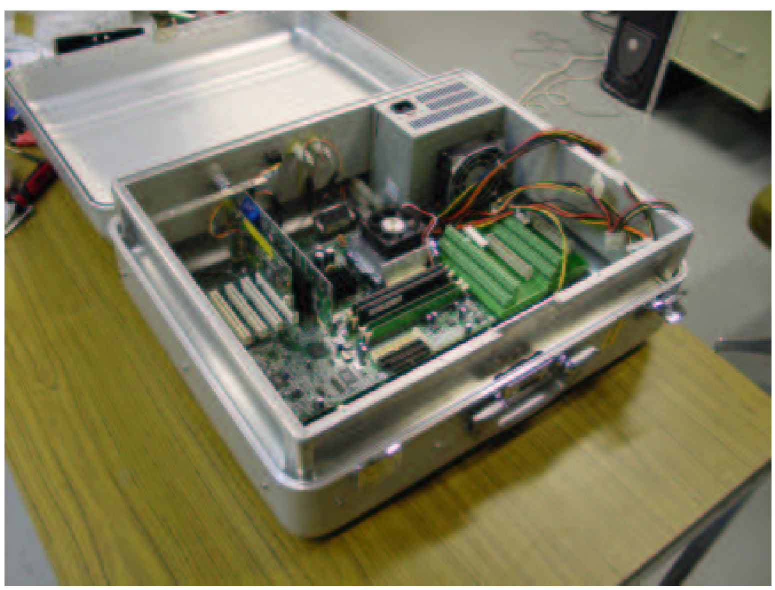

Figure 3.3: A view of the control unit with the PC platform.

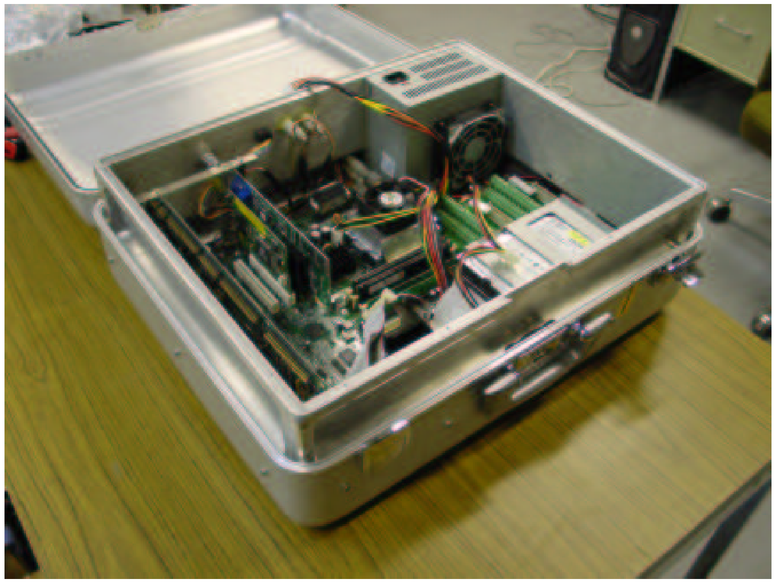

Figure 3.4: A view of the control unit with all boards installed.

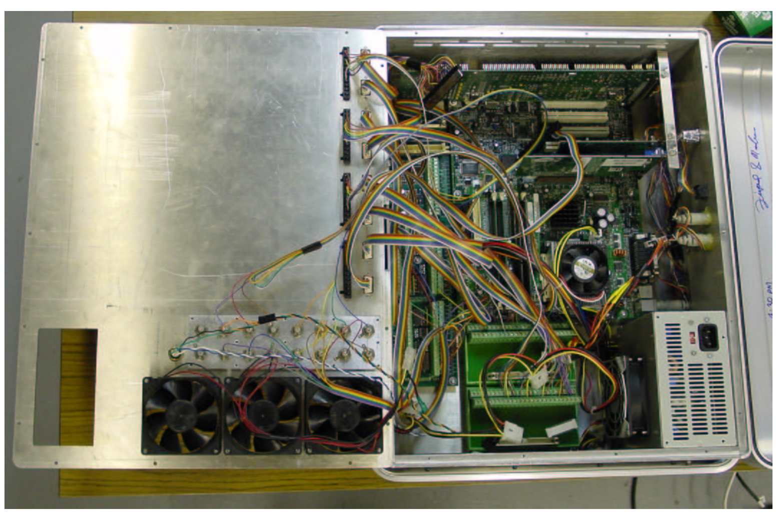

Figure 3.5: Top view of the controller with all of the components and wiring installed

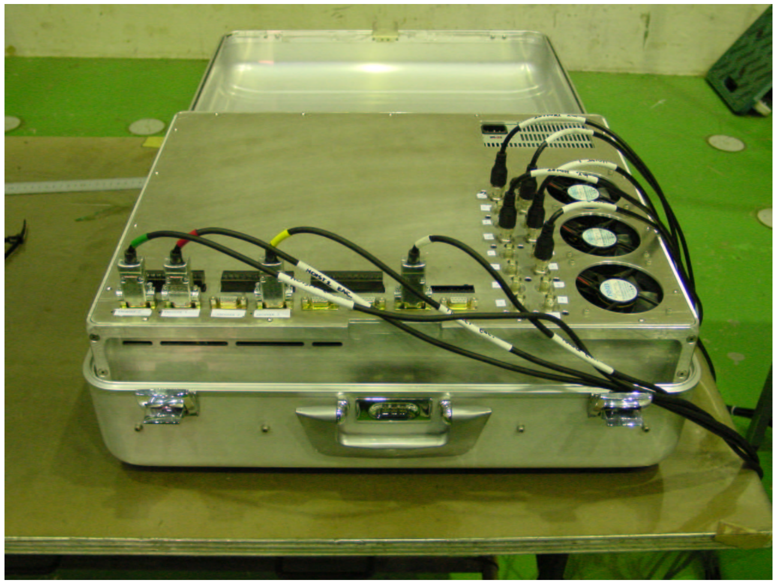

Figure 3.6: A picture of the control unit with the interface cables connected.

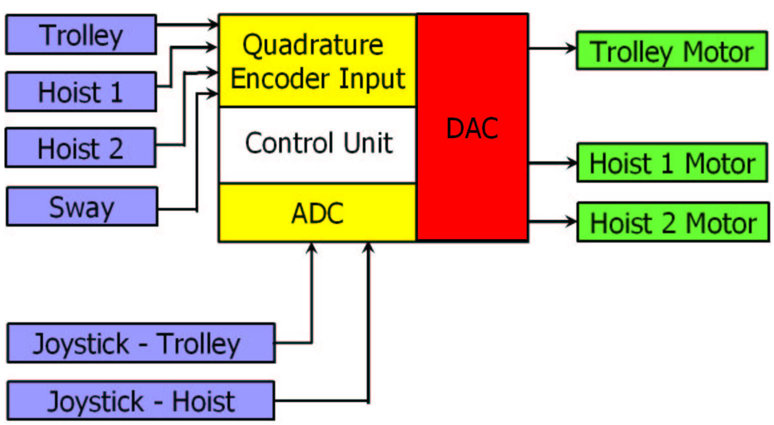

Figure 3.7: Interface diagram between the crane model and the control unit.

freedom.

The 5 m track is essentially a large balcony mounted to a wall. Underneath this balcony on rails is a large trolley that houses the hoisting motors and a camera focused on the load. The trolley is driven via a cable system where the trolley motor is mounted on one end of the rail. There, a 1:20 gearbox and a 250 mm diameter drum transfer the power from the motor to the cable driving the trolley. Due to the actual size of the trolley, the maximum traversing distance is actually 4.8 m. The motor has a built-in rotary quadrature encoder with a resolution of 512 pulses per rotation.

The two hoisting motors on the trolley work independently of each other. The two motors are configured with 1:33 gearboxes, 125 mm diameter drums, and quadrature encoders with 512 pulses per rotation. Four cables are used, two for each motor. The distance separating the hoisting cables at the trolley is 282 mm.

The four cables are then attached to the load spreader bar. IHI has a setup where the distance separating the cables at the spreader bar could be adjusted by a small motor, however for our controller the distance separating the hoisting cables at the spreader bar was set to 141 mm. The spreader bar also houses an accelerometer. Two load cells are installed on two of the hoisting cables. Unfortunately, because of the motor, accelerometer, and load cells, several very thick and heavy cables are attached to the side of the spreader bar. These cables changed the system dynamics slightly and induced some twist in the payload motion after traversing.

The load is a 65 kg weight consisting of 4 250×250 mm steel slabs, mounted to the bottom of the 15 kg spreader bar. Figure 3.8 shows the configuration of the cables to the spreader bar with the weight attached.

Driving these motors is a custom-built driving unit. The unit has external inputs for driving signals to the motors and outputs for the various sensors and encoders. The driving unit could also be used to manually drive the system via push-button controls. The unit houses the motor amplifiers, which are configured in velocity (voltage) mode.

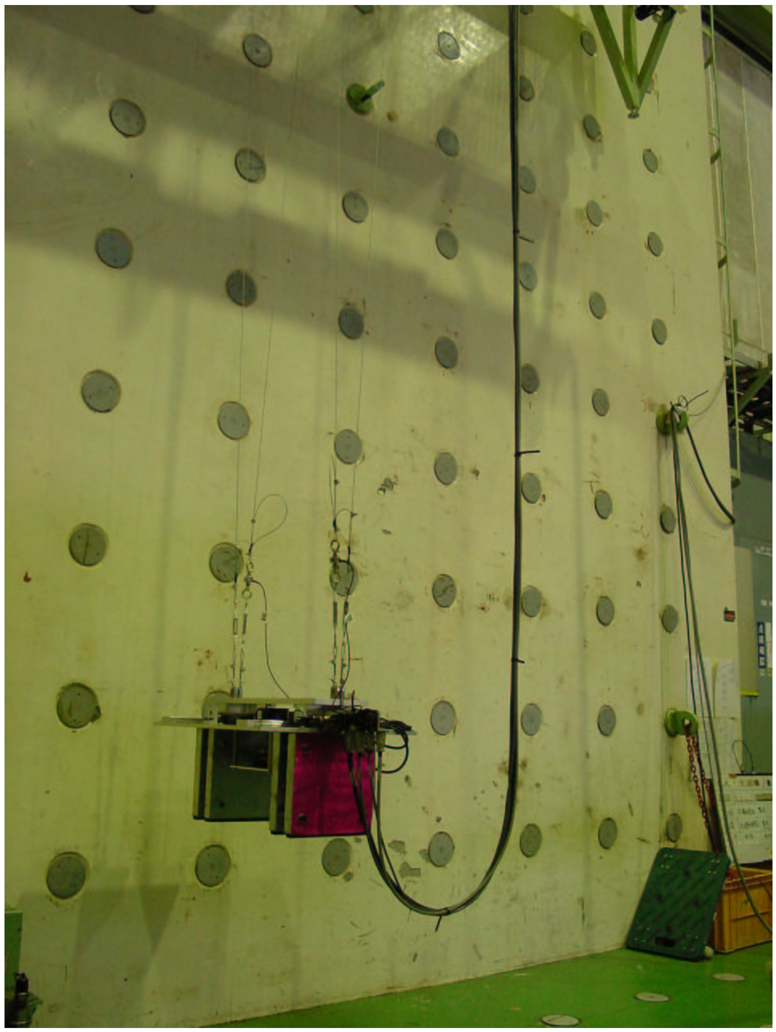

Figure 3.8: A picture of the IHI's experimental model of a container crane, spreader bar, and payload.

Chapter 4

Results

4.1 Full Scale Numerical Simulations

For the full scale container crane, the requirements of the controller are to reduce the sway motion to within 50 mm in under 5 s at the end of the transfer maneuver. This is not a simple task, as the combined load and spreader bar can be as high as 80-tons and the commanded trajectory may consist of lifting the payload 15 m, moving it 50 m, and lowering it 15 m in as fast as 21.5 s.

Three cases were simulated for the full-scale computer model of the container crane, covering typical cargo handling maneuvers. In the first case, the simulation was started with the load placed 35 m below the trolley. The load was then hoisted up to 20 m below the trolley while being traversed 50 m. The operator commanded acceleration profiles and the corresponding cargo trajectory are shown in Figure 4.1.

Figure 4.2(a) shows the controlled and uncontrolled simulations of the load sway. Figure 4.2(b) shows the controlled simulation zoomed in on the end sway. Within 3.5 s of the end of the commanded maneuver, the amplitude of the load sway of the controlled system was reduced to less than 50 mm.

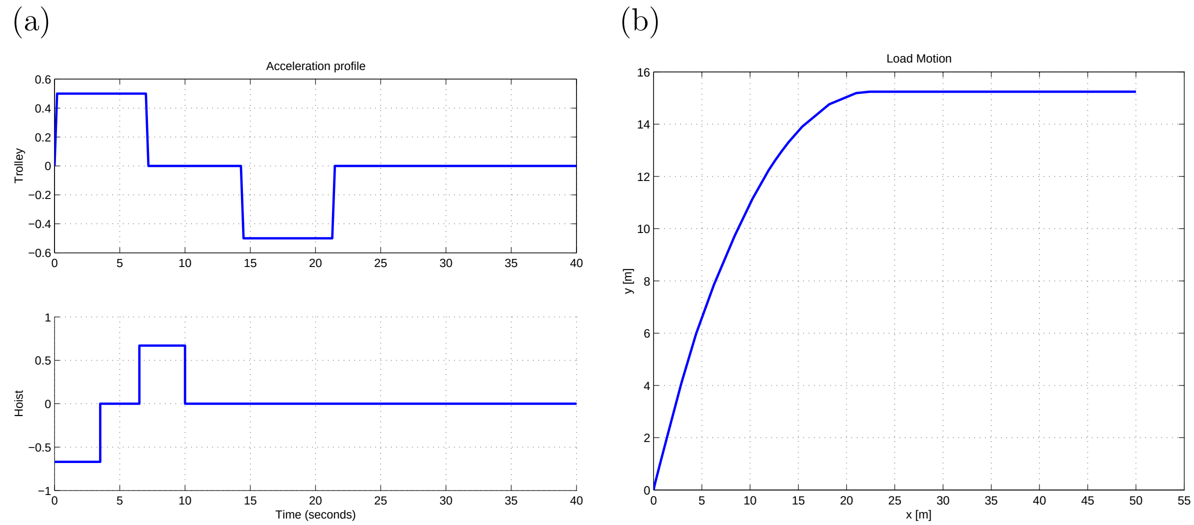

Figure 4.1: Case 1: (a) operator commanded traverse and hoist accelerations and (b) corresponding cargo trajectory.

In the second case, the simulation was started with the load 20 m below the trolley. The trolley was traversed 50 m. Near the end of the traverse motion, the load was lowered to 35 m below the trolley. The lowering motion of the cargo started during and continued after the end of the traverse motion of the trolley. The operator commanded acceleration profiles

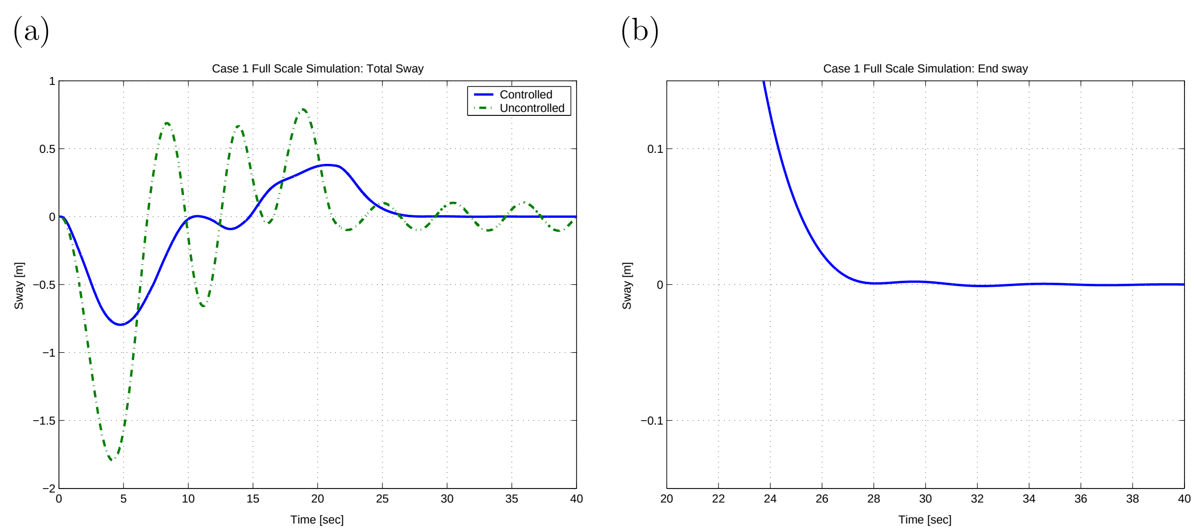

Figure 4.2: Case 1: (a) Controlled and uncontrolled load sway. (b) Controlled simulation results zoomed on the end sway.

and the corresponding cargo trajectory are shown in Figure 4.3. Figure 4.4(a) shows the load sway in the controlled and uncontrolled simulations. Figure 4.4(b) shows the controlled simulation zoomed in on the end sway. Within 4.0 s of the end of the commanded maneuver, the amplitude of the load sway in the controlled system was reduced to less than 50 mm while the load sway in the uncontrolled system continued to show a large motion.

The third case was a combination of the first and second cases. The simulation was started with the load placed 35 m below the trolley. The load was hoisted up to 20 m below the trolley while the trolley was traversed 50 m horizontally. Near the end of the traverse motion, the load was lowered to approximately 35 m below the trolley. The lowering of the cargo started during and continued after the end of the traverse motion of the trolley. The operator commanded acceleration profiles and the corresponding cargo trajectory are shown in Figure 4.5. The simulation results for the load sway in the controlled and uncontrolled cases are shown in Figure 4.6(a). Figure 4.6(b) shows the controlled simulation zoomed in on the end sway. As in the previous two cases, the load sway of the controlled system was significantly reduced to less than 50 mm within 4.0 s of the end of the commanded trolley maneuver. However, the load sway in the uncontrolled system continued to show a large

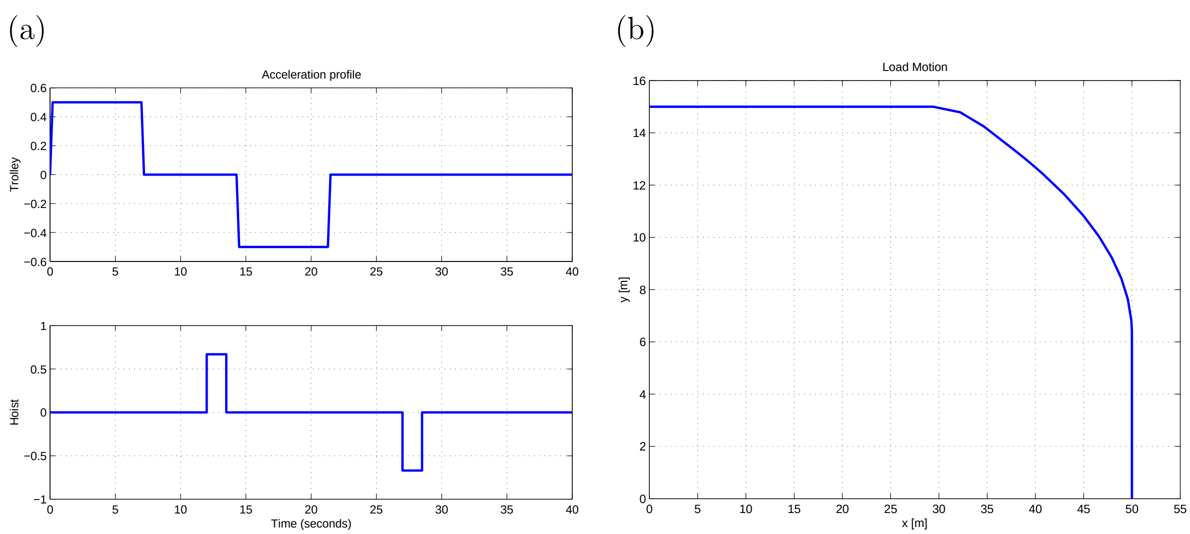

Figure 4.3: Case 2: (a) operator commanded traverse and hoist accelerations and (b) corresponding load trajectory.

(a) (b)

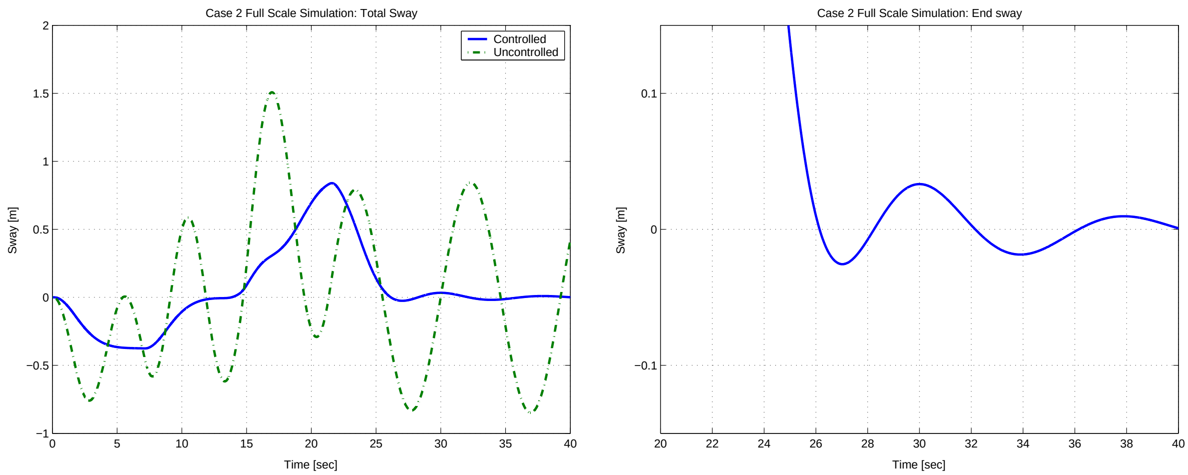

Figure 4.4: Case 2: (a) Controlled and uncontrolled load sway. (b)Controlled simulation results zoomed on the end sway.

(a) (b)

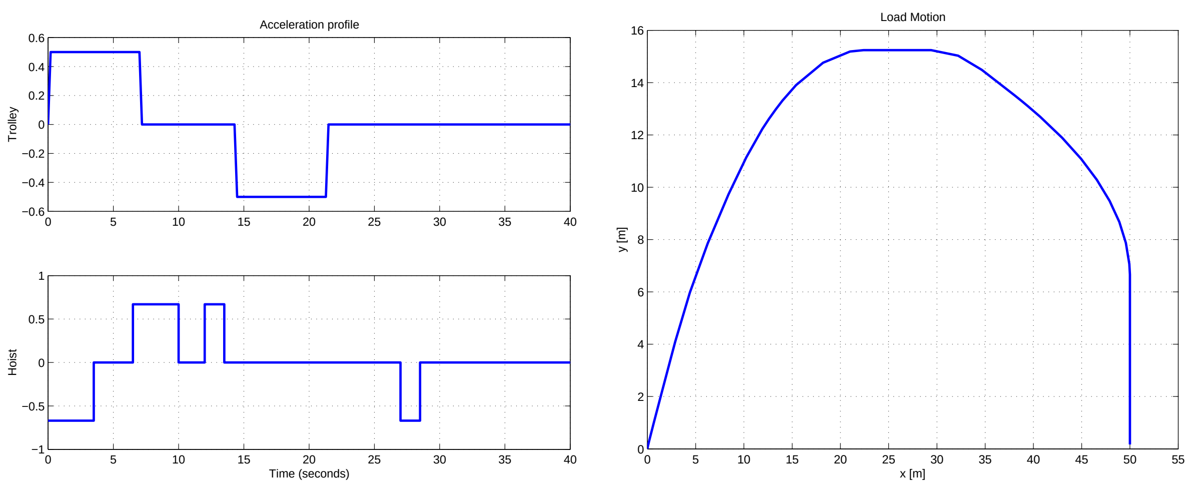

Figure 4.5: Case 3: (a) operator commanded traverse and hoist accelerations and (b) corresponding load trajectory.

motion.

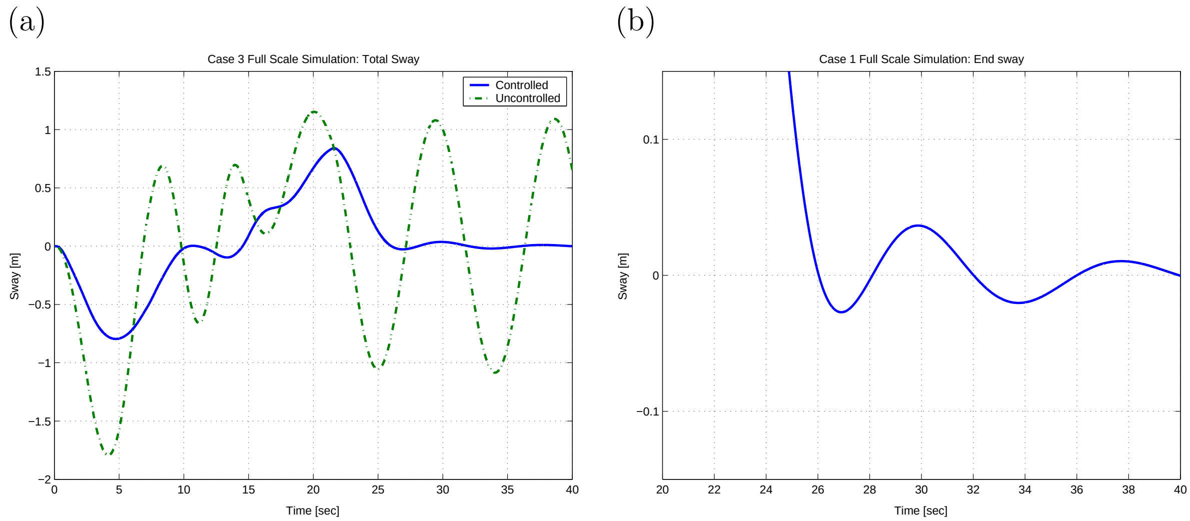

Figure 4.6: Case 3: (a) Controlled and uncontrolled load sway.(b) Controlled simulation results zoomed on the end sway.

4.2 1/10th Scale Model Numerical and Experimental Results

For the 1/10th scale model, the controller needed to dampen out the sway amplitude to under 5.0 mm within 1.6 s of the end of the transfer maneuver. In this case, the load was lifted and lowered up from a position 3.5 m below the trolley 1.5 m, while being traversed 4.5 m (due to physical track length of the model) in 6.5 s. Six test cases were designed to test the capability of the controller. Each of the tests were based on real-life operations of container cranes. In each test, the controller performance was tested with and without a payload on the spreader bar.

4.2.1 Case 1

The commanded acceleration, velocity, and position profiles for Case 1 are shown in Figure 4.7. The trolley was accelerated at a rate of 0.5 m/s^2 to a maximum velocity of 1.0 m/s. The trolley coasted at this velocity for 2.5 s. After 4.5 s from the beginning of the maneuver,

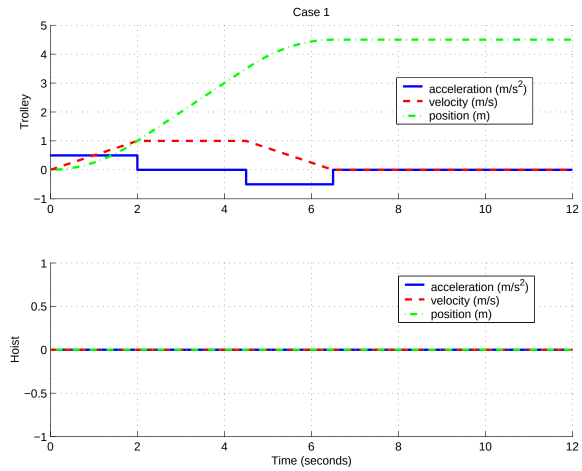

Figure 4.7: Tested profile 1.

the trolley was decelerated at a rate of 0.5 m/s^2 for 2.0 s. In the end, the trolley had moved 4.5 m in 6.5 s. The hoist was kept constant at 3.5 m below the trolley.

Figure 4.8(a) shows the controlled and uncontrolled simulations and experimental sway results for Case 1 with a payload. The controlled simulation and experimental data are a very close match throughout the entire transfer maneuver. Figure 4.8(b) shows a zoom on the load way after 6.0 s of the maneuver start; the sway was brought to under 5 mm at 8.2 s or 1.6 s after the end of the maneuver. Also, due to the interaction of the heavy cables shown in Figure 3.8, the load began to twist slightly causing a false sway reading.

Figure 4.9(a) shows the experimental results for Case 1 without a payload. Figure 4.9(a) shows a zoom on the results near the end of the maneuver. Since the cables shown in Figure 3.8 were heavy compared to the spreader bar, the controller was not able to reduce the sway motion at the end of the maneuver. However the twisting motion of the payload persisted. This twisting motion resulted in an inaccurate sway reading since the sway angle sensor was mounted on one side of the hoisting cables.

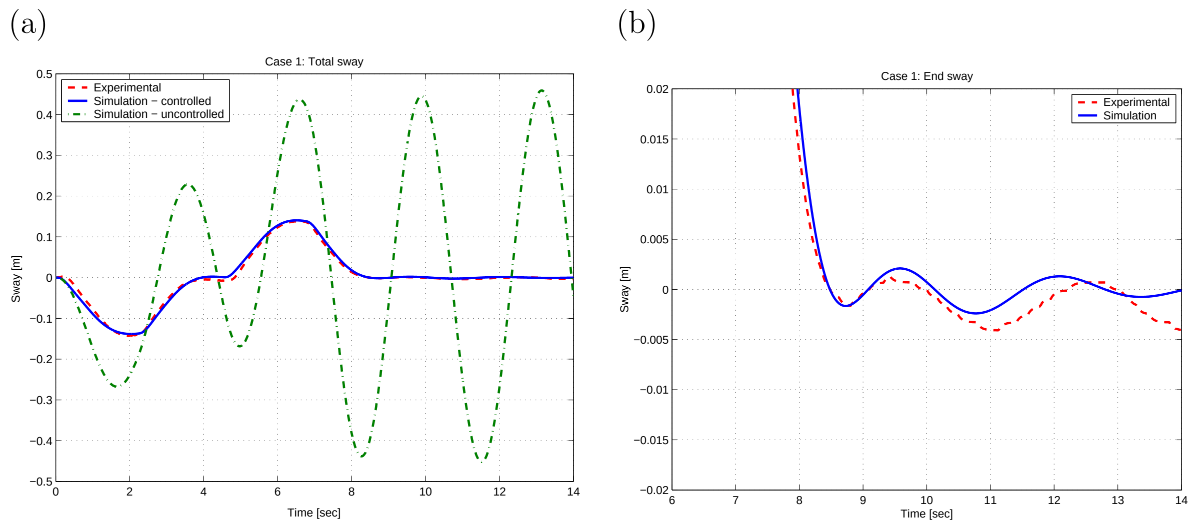

Figure 4.8: (a) The simulation and experimental results for Case 1 and (b) a zoom on the simulation and experimental results for Case 1, loaded.

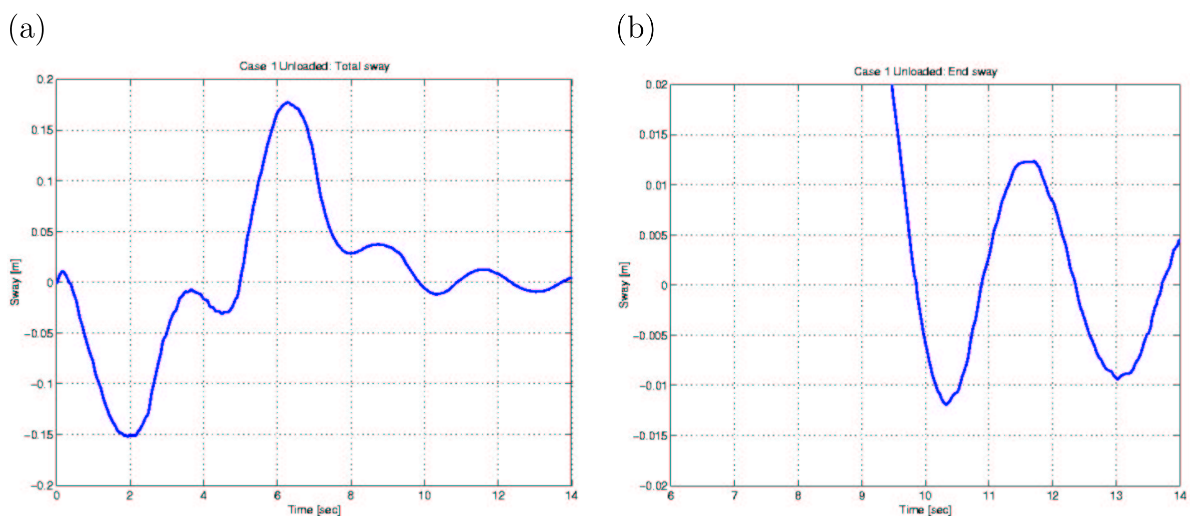

Figure 4.9: (a) The experimental results for Case 1 and (b) a zoom on the experimental results for Case 1, unloaded.

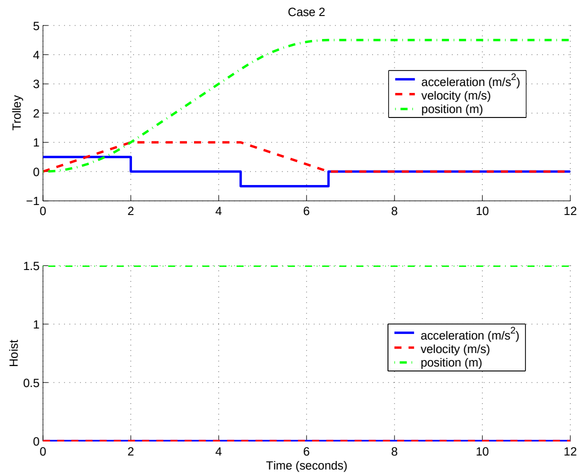

Figure 4.10: Tested profile 2.

4.2.2 Case 2

The commanded acceleration, velocity, and position profiles for Case 2 are shown in Figure 4.10. The trolley was accelerated at a rate of 0.5 m/s^2 to a maximum velocity of 1.0 m/s. The trolley coasted at this velocity for 2.5 s. After 4.5 s from the beginning of the maneuver, the trolley was decelerated at a rate of 0.5 m/s^2 for 2.0 s. In the end, the trolley moved 4.5 m in 6.5 s. The hoist was held constant 2.0 m below the trolley.

Figure 4.11(a) shows the controlled and uncontrolled simulations and experimental sway results for Case 2 with a payload. The controlled simulation and experimental data are a very close match throughout the entire maneuver. Figure 4.11(b) shows a zoom on the results at the end of the operation. It can be observed that the controller met the criterion of reducing the sway to below 5 mm in under 1.6 s. In fact, the sway is almost negligible in this case, but, due to the heavy cables, there are some aperiodic oscillations.

Figure 4.12(a) shows the experimental results for the unloaded case. Figure 4.12(b) shows a zoom on the results near the end of the maneuver.

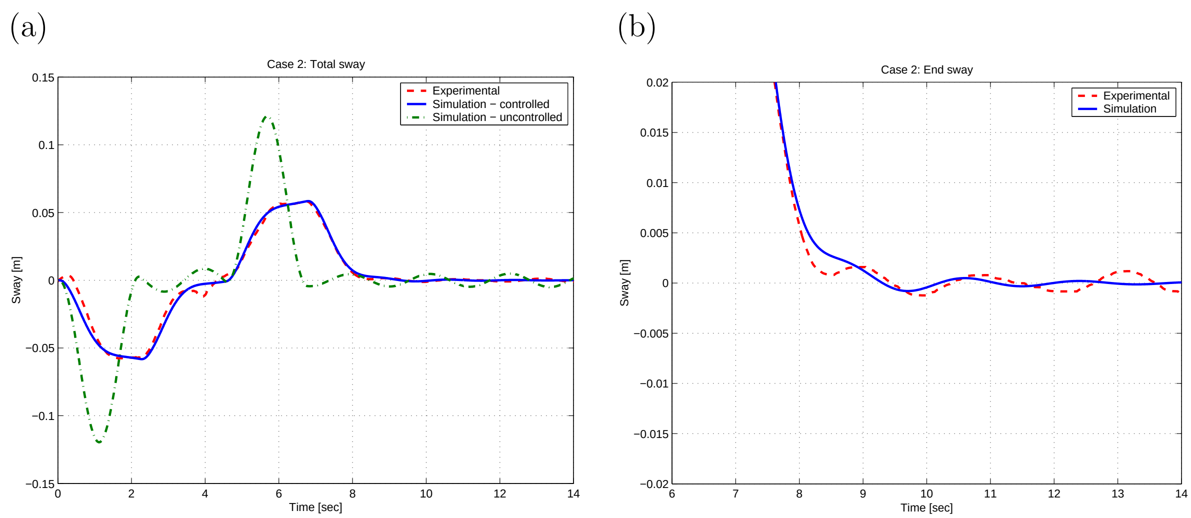

Figure 4.11: (a) The simulation and experimental results for Case 2 and (b) a zoom on the simulation and experimental results for Case 2, loaded.

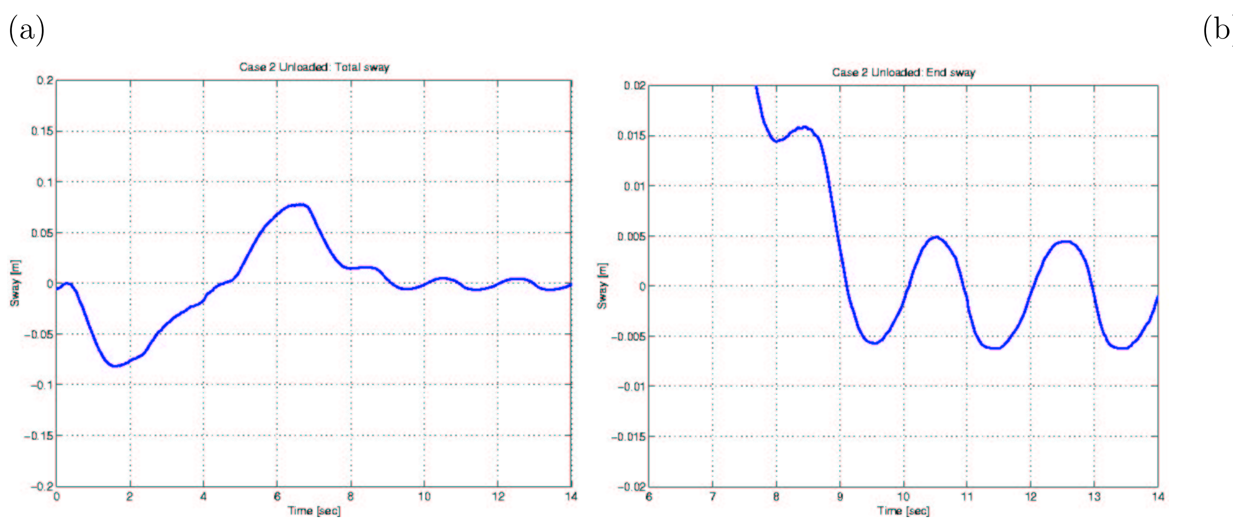

Figure 4.12: (a) The experimental results for Case 2 and (b) a zoom on the experimental results for Case 2, unloaded.

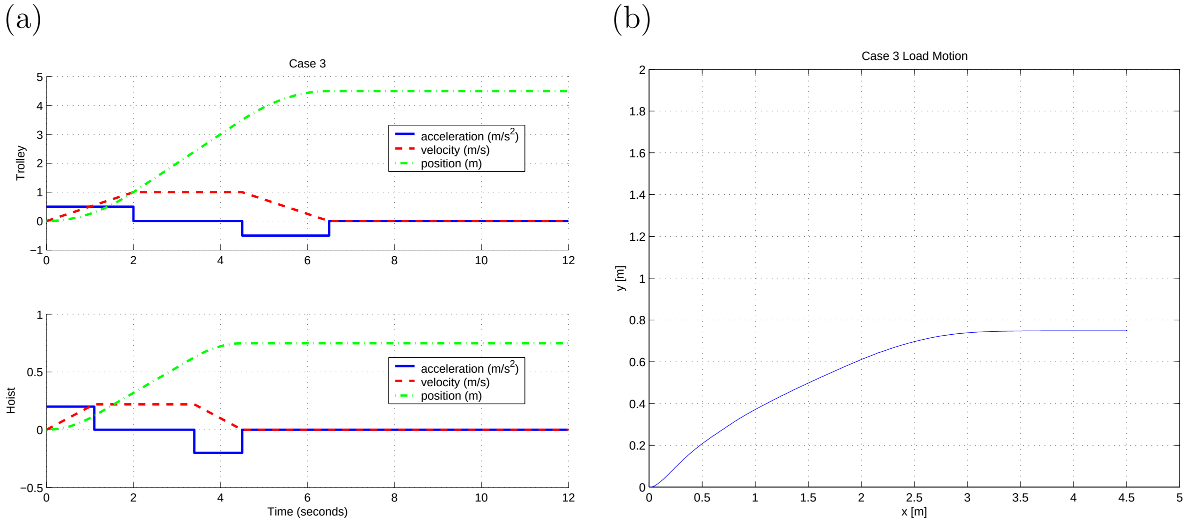

Figure 4.13: (a) Tested profile 3. (b) Commanded load trajectory.

4.2.3 Case 3

The commanded acceleration, velocity, and position profiles for Case 3 are shown in Figure 4.13(a). Figure 4.13(b) shows an x-y plot of the commanded load trajectory. The trolley was accelerated at a rate of 0.5 m/s^2 to a maximum velocity of 1.0 m/s. The trolley coasted at this velocity for 2.5 s. After 4.5 s from the beginning of the maneuver, the trolley was decelerated at a rate of 0.5 m/s^2 for 2.0 s. In the end, the trolley moved 4.5 m in 6.5 s.

The hoist was accelerated at a rate of 0.2 m/s^2 for 1.1 s to a maximum velocity of 0.22 m/s. Then the hoist was driven at that velocity for 2.3 s. Finally, the hoist was decelerated at a rate of 0.2 m/s^2 for 1.1 s where the payload reached 0.75 m in height where it remained constant for the duration of the maneuver. .

Figure 4.14(a) shows the controlled and uncontrolled simulations and experimental sway results for Case 3 with the payload. The controlled simulation and experimental data are a very close match throughout maneuver. Figure 4.14(b) shows a zoom on the results near the end of the maneuver. It can be observed that the controller met the criterion of reducing sway below 5 mm in under 1.6 s. The experimental sway is larger than what was expected

(a) (b)

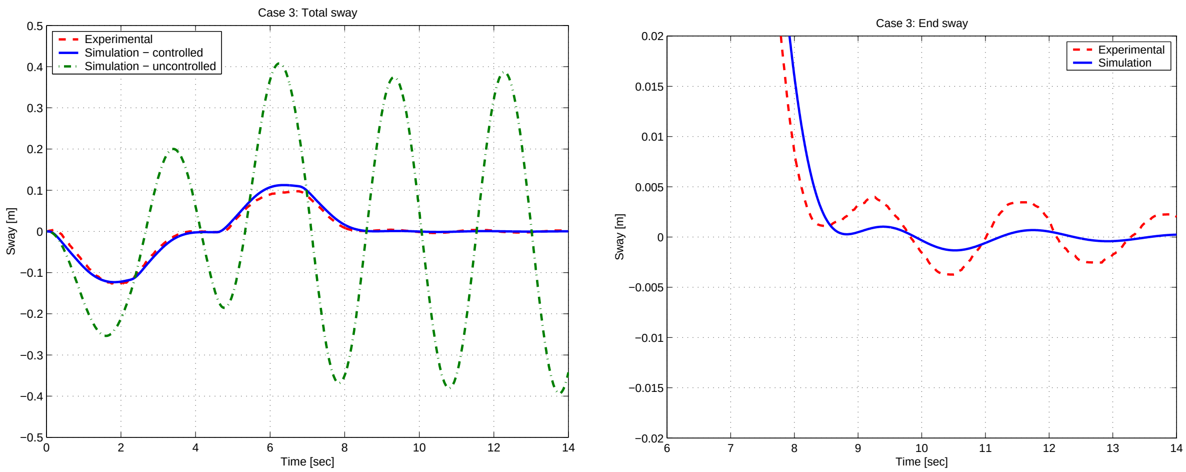

Figure 4.14: (a) The simulation and experimental results for Case 3 and (b) a zoom on the simulation and experimental results for Case 3, loaded.

from the simulation and there appears to be a slight drift in the sway motion. Unfortunately, it is difficult to tell if this is from the controller or from the induced twist.

This case was not tested unloaded.

4.2.4 Case 4

The commanded acceleration, velocity, and position profiles for Case 4 are shown in Figure 4.15(a). Figure 4.15(b) shows an x-y plot of the commanded load trajectory. The trolley was accelerated at a rate of 0.5 m/s^2 to a maximum velocity of 1.0 m/s. The trolley coasted at that velocity for 2.5 s. After 4.5 s from the beginning of the maneuver, the trolley was decelerated at 0.5 m/s^2 for 2.0 s. In the end, the trolley moved 4.5 m in 6.5 s.

The hoist was accelerated at a rate of 0.4 m/s^2 for 1.1 s to a maximum velocity of 0.44 m/s. Then the hoist was driven at that velocity for 2.3 s. Finally, the hoist was decelerated at a rate of 0.4 m/s^2 for 1.1 s where the payload had been lifted 1.5 m and the hoist was held constant 2.0 m below the trolley.

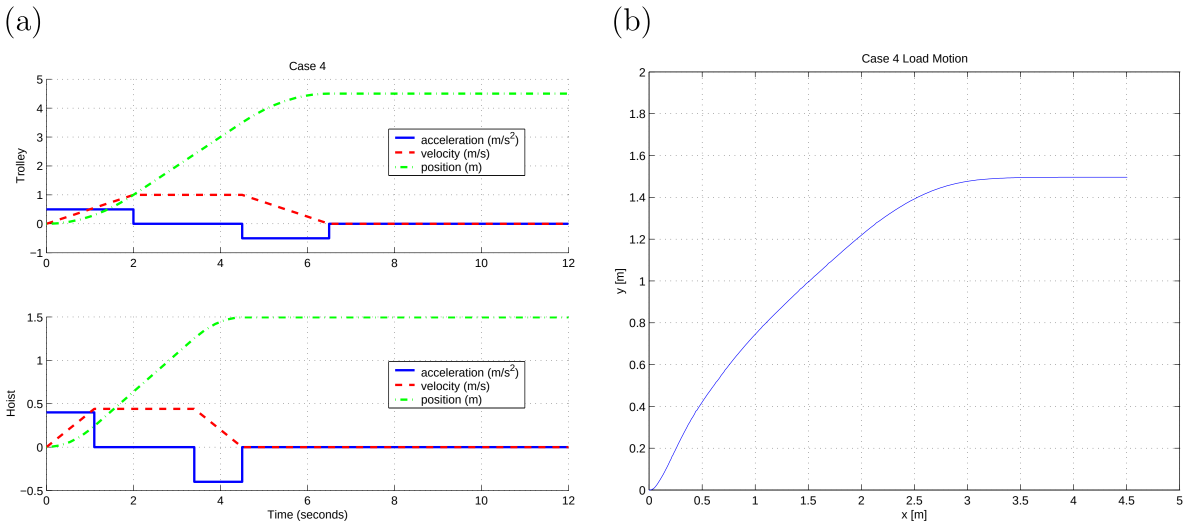

Figure 4.15: (a) Tested profile 4. (b) Commanded load trajectory.

Figure 4.16(a) shows the controlled and uncontrolled simulations and experimental sway results for Case 4 with a payload. The controlled simulation and experimental data are a very close match throughout the maneuver. Figure 4.16(b) shows a zoom on the results at the end of the maneuver. It can be observed that the system met the criterion of reducing sway under 5 mm in under 1.6 s. In fact, the end sway motion for this case is almost

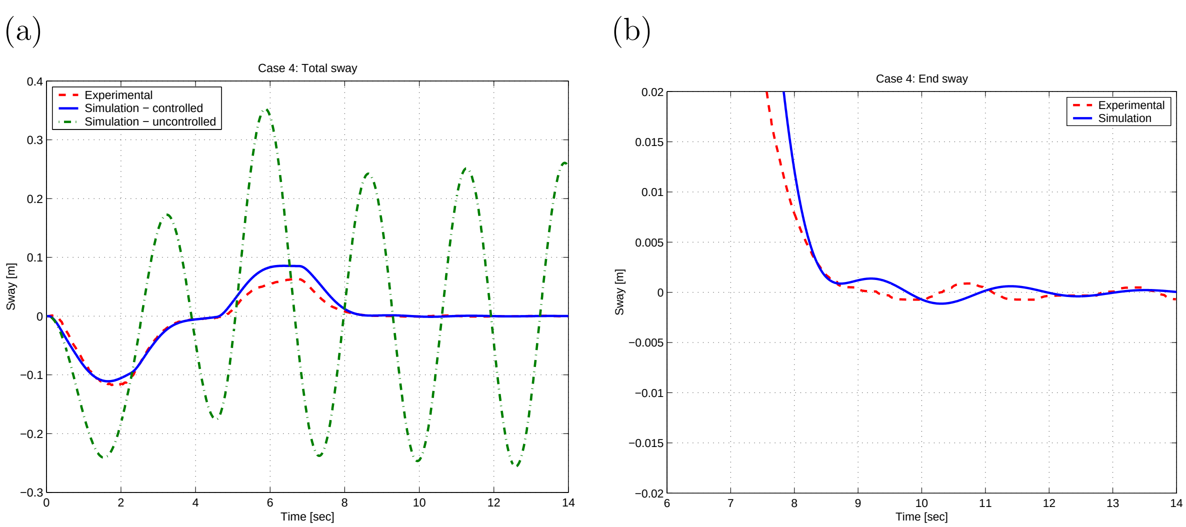

Figure 4.16: (a) The simulation and experimental results for Case 4 and (b) a zoom on the simulation and experimental results for Case 4, loaded.

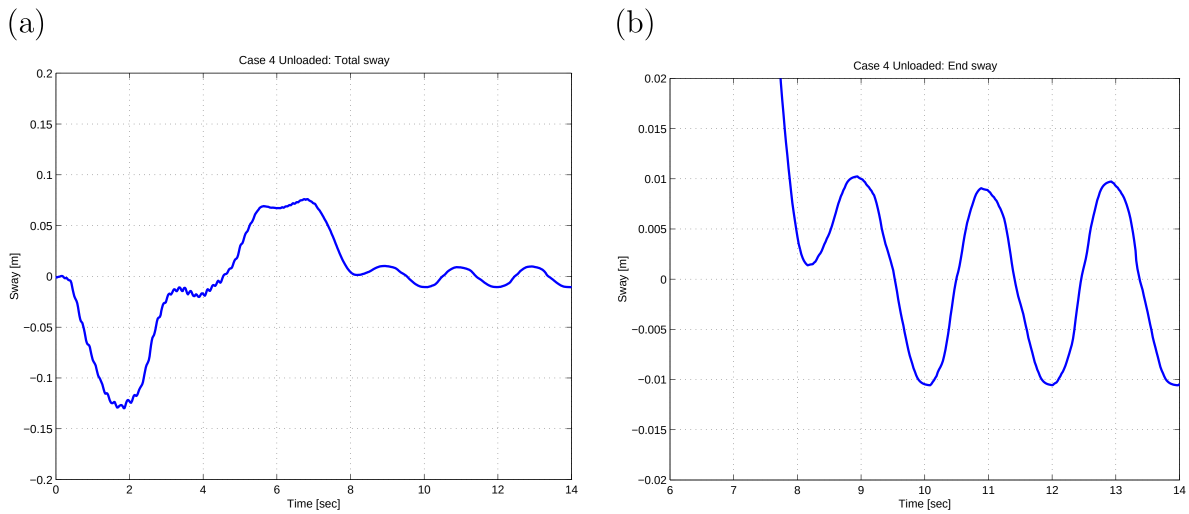

Figure 4.17: (a) The experimental results for Case 4 and (b) a zoom on the experimental results for Case 4, unloaded.

negligible.

Figure 4.17(a) shows the experimental results for the unloaded case. Figure 4.17(b) shows a zoom on the results at the end the operation. The end sway for this motion never went under 5 mm, but it did stay within 10 mm due to the twist motion of the payload.

4.2.5 Case 5

The commanded acceleration, velocity, and position profiles for Case 5 are shown in Figure 4.18(a). Figure 4.18(b) shows an x-y plot of the commanded load trajectory. The trolley was accelerated at a rate of 0.5 m/s^2 to a maximum velocity of 1.0 m/s. The trolley coasted at this velocity for 2.5 s. After 4.5 s from the beginning of the maneuver, the trolley was decelerated at 0.5 m/s^2 for 2.0 s. In the end, the trolley moved 4.5 m in 6.5 s.

The hoist began at 2.0 m below the trolley. Then, at 5.0 s, the hoist was accelerated down at a rate of 0.4 m/s^2 until the velocity reached 0.44 m/s. The velocity was held constant for 2.3 s. At 8.4 s from the beginning of the maneuver, the hoist was decelerated at a rate of 0.4 m/s^2 for 1.1 s, where its motion stopped. Overall, the hoist was lowered 1.5 m to a

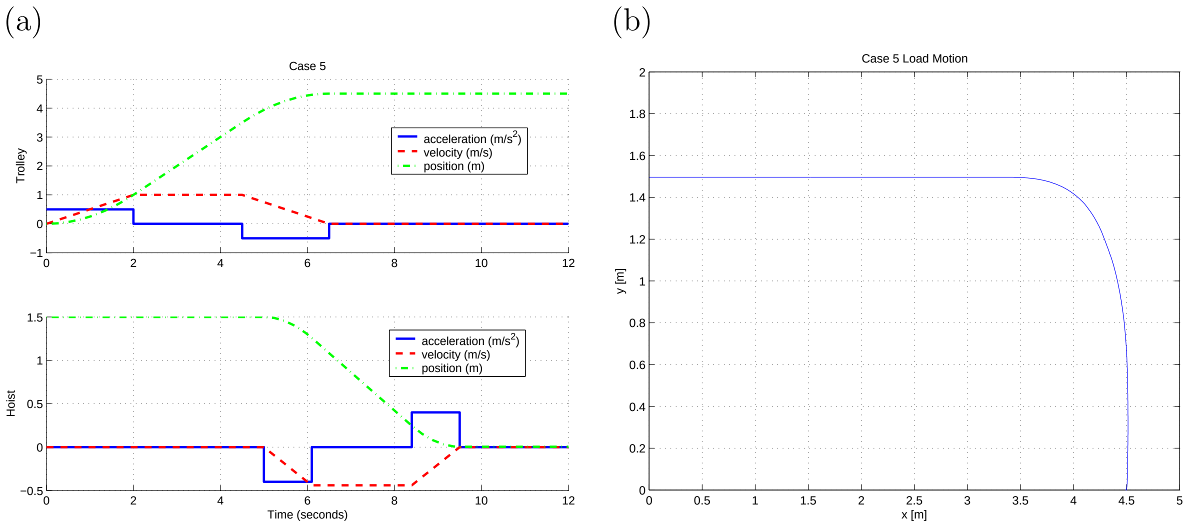

Figure 4.18: (a) Tested profile 5. (b) Commanded load trajectory.

position 3.5 m below the trolley. The motion ceased in the system at 9.1 s, instead of the usual 6.8 s.

Figure 4.19(a) shows the uncontrolled and controlled simulation and experimental sway results for Case 5 with the payload. The controlled simulation and experimental data are a very close match throughout the maneuver. Figure 4.19(b) shows a zoom on the sway at the end of the maneuver. It can be observed that the system met the criterion of reducing sway under 5 mm in under 1.6 s after motion. The end sway is very small, however there is some aperiodic oscillations, which indicate a twisting motion of the load.

Figure 4.20(a) shows the experimental results for the unloaded case. Figure 4.20(b) shows a zoom on the sway near the end of the operation. In the unloaded case, the extra "chatter" seen is due to badly tuned amplifiers. The motors were driving the load faster than it could accelerate down. Hence, there was some slack in the cable which caused the encoder measuring the angle to fluctuate. However, the end sway motion was brought under 5 mm within 4 s.

(a) (b)

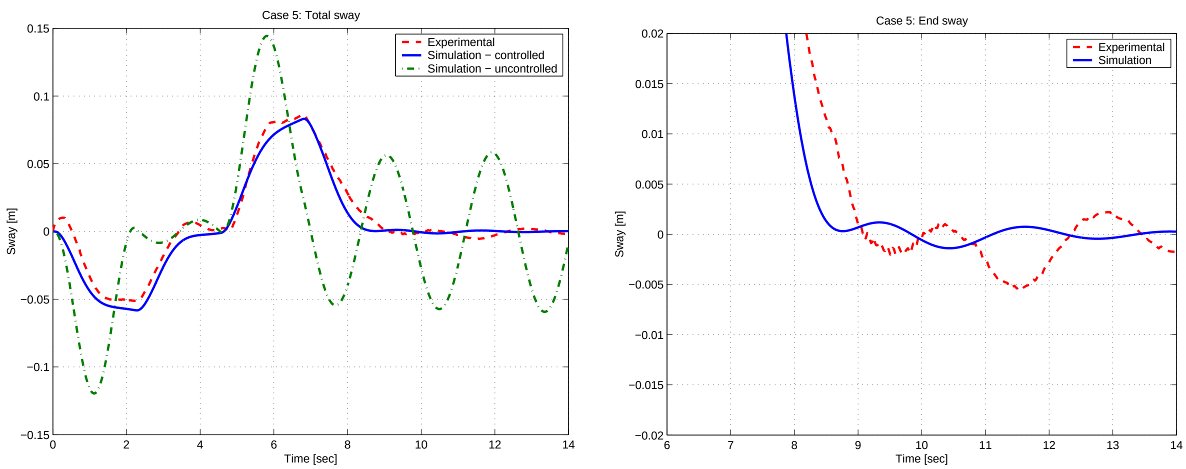

Figure 4.19: (a) The simulation and experimental results for Case 5 and (b) a zoom on the simulation and experimental results for Case 5, loaded.

(a) (b)

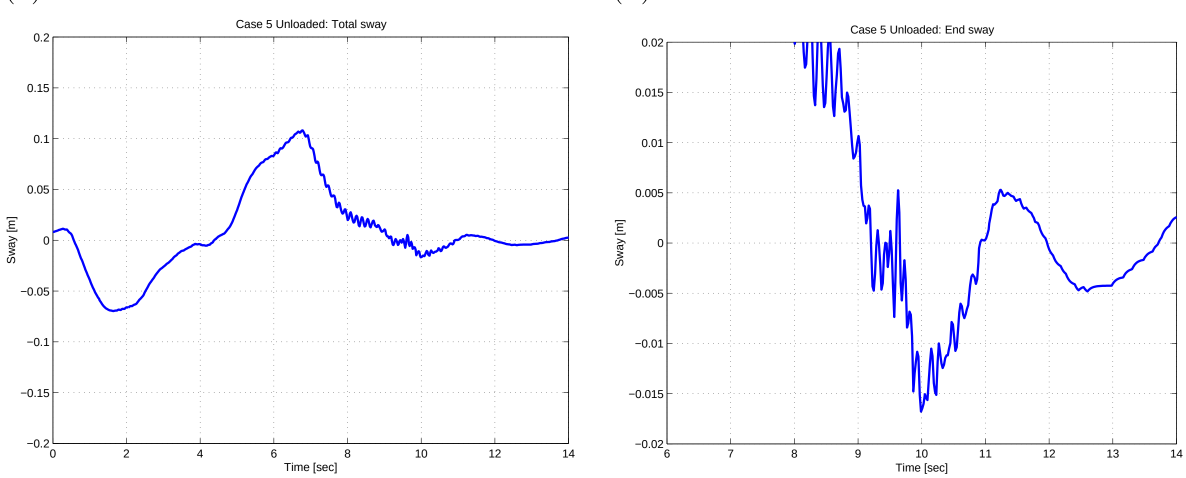

Figure 4.20: (a) The experimental results for Case 5 and (b) a zoom on the experimental results for Case 5, unloaded.

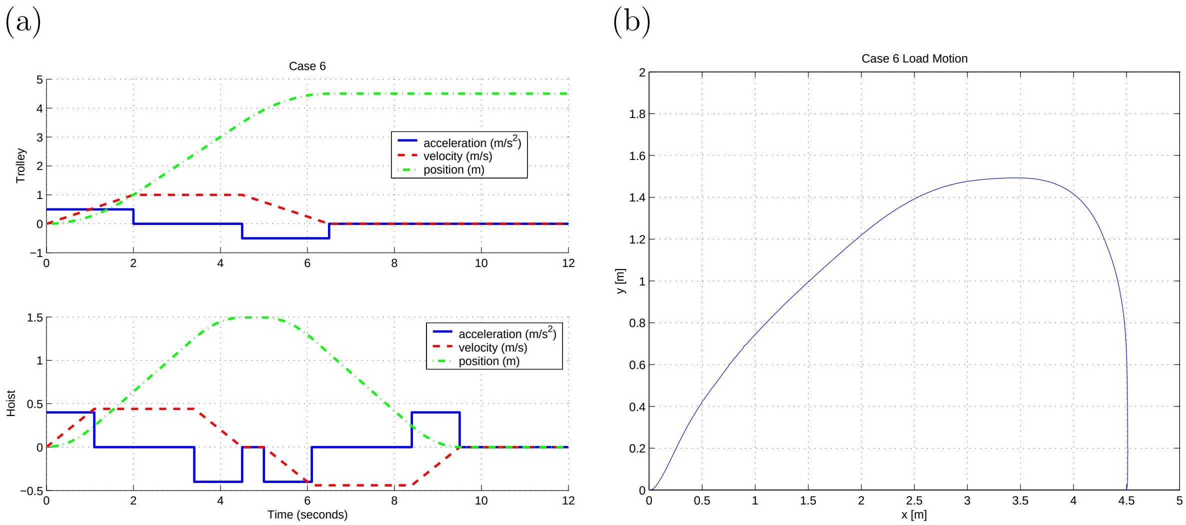

Figure 4.21: (a) Tested profile 6. (b) Commanded load trajectory.

4.2.6 Case 6

The commanded acceleration, velocity, and position profiles for Case 6 are shown in Figure 4.21(a). Figure 4.21(b) shows an x-y plot of the commanded load trajectory. The trolley was accelerated at a rate of 0.5 m/s^2 to a maximum velocity of 1.0 m/s. The trolley coasted at this velocity for 2.5 s. After 4.5 s from the beginning of the maneuver, the trolley was decelerated at a rate of 0.5 m/s^2 for 2.0 s. In the end, the trolley moved 4.5 m in 6.5 s.

The hoist motion in Case 6 was a combination of the hoisting actions of Case 4 and Case 5. The hoist was moved up 1.5 m and then it was lowered 1.5 m; the profile for Case 4 was used to move the load up, and the profile for Case 5 was used to move the load down.

Figure 4.22(a) shows the uncontrolled and controlled simulations and experimental sway results for Case 6 with the payload. The controlled simulation and experimental data are a very close match throughout the maneuver. Figure 4.22(b) shows a zoom in on the sway near the end of the maneuver. Unfortunately, for this case, the end sway did not meet the requirements in experimental results. Note, also, that there is more negative sway than positive sway, which is an indication that there is some twisting motion in the load.

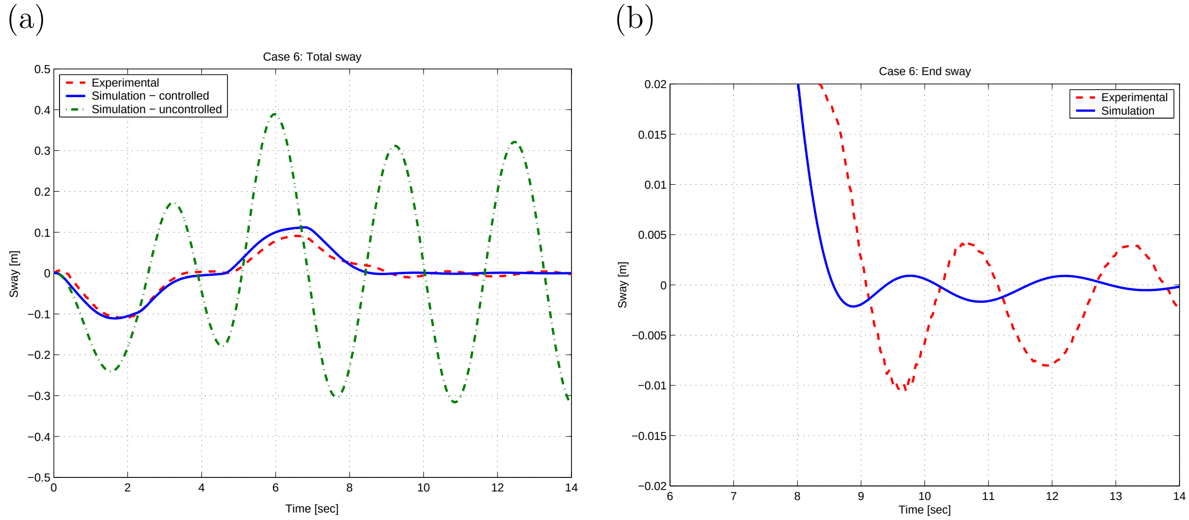

Figure 4.22: (a) The simulation and experimental results for Case 6 and (b) a zoom on the simulation and experimental results for Case 6, loaded.

Figure 4.23(a) shows the experimental results for the unloaded case. Figure 4.23(b) shows a zoom in on the sway at the end of the maneuver. There was quite a bit of “chatter” in this case. Once again, due to the badly tuned amplifiers, the load was being driven faster than it could be accelerated down, hence there was some slack in the cable causing the sensor to wiggle. Unfortunately, the end sway did not decay below the 5 mm mark.

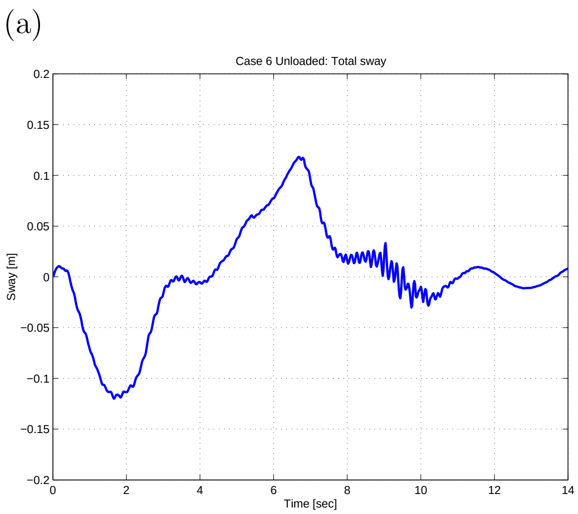

Figure 4.23: (a) The experimental results for Case 6 and (b) A zoom on the experimental results for Case 6, unloaded.

Chapter 5

Conclusions

5.1 Summary

More and more container cranes are being pushed to faster speeds and higher turn around rates. The latest requirement for such a crane is to operate by moving an 80-ton container and spreader bar 50 m in 21.5 s. Then, within 5 s of the end of the transfer maneuver, the sway needs to settle down to within 50 mm.

To solve the crane sway problem, we derived a controller based on the delayed feedback controller of Henry, et al. (2001). Numerical simulations were conducted, which showed that the controller met the above stated requirements.

In order to validate the simulation results, we implemented the controller in hardware and applied it to a 1/10th scale model of a container crane. The requirements for the full scale translate to the 1/10th scale model as traversing an 80-kg load 5 m in 6.8 s and reducing the sway to less than 5 mm within 1.6 s. Some difficulty in the experimental setup prevented the controller from meeting the requirements in some of the test cases. Unfortunately, the usable track was only 4.5 m instead of 5 m. Also, several heavy cables were attached to the payload, causing a twisting motion in the payload that the controller was not designed to handle.

Lastly, as a validation of the true performance of the controller, a manual mode of operation was implemented. The manual mode of operation is a very good test as the operator inputs are random signals. Also, no two operators move the crane and hoist the payload in the same way. During the experimental tests, over 30 different people attempted to destabilize the system operating in the manual mode. None of them succeeded.

5.2 Recommendations for Future Work

One recommendation for future work is to build a model container crane that avoids the design flaws that were encountered with IHI's, most notably the external cables that affected the system dynamics and caused a twisting motion. It is also recommended to increase the usable track length more than 4.5 m.

Another recommendation for future work is to implement the controller using a better hardware setup. The custom box took a lot of work to fit everything into the suitcase. Also, due to some issues with the Aerotech U500 and operating system, the sampling times were not as good as planned. A timer board should be integrated with the setup to obtain improved signal sampling.

Finally, implementing and testing the controller on a full-scale container crane would be the best way to validate the controller performance.

References

Abdel-Rahman, E. M., Nayfeh, A. H., and Masoud, Z. N. (2002) "Dynamics and Control of Cranes: A Review." *Journal of Vibration and Control*, Accepted for publication.

Alsop, C. F., Forster, G. A., and Holmes, F. R. (1965) "Ore Unloader Automation - A Feasibility Study." *Proceedings of IFAC on Systems Engineering for Control Systems*, Tokyo, Japan, 295-305.

Burg, T., Dawson, D., Rahn, C., and Rhodes, W. (1996) "Nonlinear Control of an Overhead Crane Via the Saturating Control Approach of Teel." *Proceedings of the 1996 IEEE International Conference on Robotics and Automation*, 3155-3160.

d'Andrea-Novel, B. and Levine, J. (1989) "Modeling and Nonlinear Control of an Overhead Crane." *Proceedings of the International Symposium MTNS-89*, 2:523-529.

Dadone, P. and VanLandingham, H. F. (2002) "Load Transfer Control for a Gantry Crane with Arbitrary Delay Constraints." *Journal of Vibration and Control*, in press.

Henry, R. J., Masoud, Z. N., Nayfeh, A. H., and Mook, D. T. (2001) "Cargo Pendulation Reduction on Ship-Mounted Cranes Via Boom-Luff Angle Actuation." *Journal of Vibration and Control*, 7:1253-1264.

Jones, J. F. and Petterson, B. J. (1988) "Oscillation Damped Movement of Suspended Objects." *Proceedings of the IEEE International Conference on Robotics and Automation,* Philadelphia, PA, 2:956-962.

Masoud, Z. N., Nayfeh, A. H., and Al-Mousa, A. (2002) "Delayed Position-Feedback Controller for the Reduction of Payload Pendulations of Rotary Cranes." *Journal of Vibration and Control*, Accepted for publication.

Masoud, Z. N. and Nayfeh, A. H. (2020) "Sway Reduction on Container Cranes Using Delayed Feedback Controller." *Nonlinear Dynamics*, Submitted for publication.

Masoud, Z. N., Nayfeh, A. H., and Mook, D. T. (2002) "Cargo Pendulation Reduction of Ship-Mounted Cranes." Submitted for publication, Nonlinear Dynamics.

Michelsen, F. C. and Coppens, A., (1988), "On the Upgrading of SSCV Hermod to Increase its Lifting Capacity and the Dynamics of Heavy-lift Operations," *Proceedings of the 20th Annual Offshore Technology Conference,* Houston, TX, OTC 5820.

Noakes, M. W. and Jansen, J. F. (1990) "Shaping Inputs to Reduce Vibration for Suspended Payloads." *Proceedings of the 4th ANS Topical Meeting on Robotics and Remote Systems,* Albuquerque, NM, 141-150.

Noakes, M. W. and Jansen, J. F. (1992) "Generalized Inputs for Damped-Vibration Control of Suspended Payloads." *Robotics and Autonomous Systems*, 10:199–205.

Noakes, M. W., Petterson, B. J., and Werner, J. C. (1990) "An Application of Oscillation Damped Motion for Suspended Payloads to the Advanced Integrated Maintenance System." *Proceedings of the 38th Conference on Remote Systems Technology,* San Francisco, CA, 1:63-68.

Parker, G., Groom, K., Hurtado, J., Feddema, J., Robinett, R., and Leban, F. (1999) "Experimental Verification of a Command Shaping Boom Crane Control System." *Proceedings of the American Control Conference*, 86-90.

Parker, G., Petterson, B., Dohrmann, C., and Robinett, R. (1995) "Command Shaping for Residual Vibration Free Crane Maneuvers." *Proceedings of the American Control Conference*, 934-938.

Parker, G., Robinett, R., Driessen, B., and Dohrmann, C. (1996) "Operator-in-the-Loop Control of Rotary Crane." *Proceedings of the SPIE Conference*, 2721:364-372.

Patel, M., Brown, D., and Witz, J. (1987) "Operability Analysis for a Monohull Crane Vessel." *Transactions of the Royal Institute of Naval Architects*, 129:103-113.

Singhose, W. E., Porter, L. J., and Seering, W. P. (1997) "Input Shaped Control of a Planar Crane with Hoisting." *Proceedings of the American Control Conference,* Albuquerque, NM, 97-100.

Todd, M. D., Vohra, S. T., and Leban, F., (1997), "Dynamical Measurements of Ship Crane Load Pendulation," in *Oceans'97 MTS/IEEE: Conference Proceedings,* Vol. 2, Halifax, Canada, pp. 1230–1236.

van den Boom, H. J. J., Coppens, A., Dallinga, R. P., and Pijfers, J. G. L., (1987), "Motions and Forces During Heavy Lift Operations Offshore," in *Developments in Marine Technology, Proceedings of a Workshop on Floating Structures and Offshore Operations* Vol. 4, Wageningen, The Netherlands, 4: 51–61.

Virkkunen, J. and Marttinen, A. (1988)"Computer Control of a Loading Bridge." *Proceedings of the IEE International Conference: Control'88,* Oxford, UK, 484–488.

Willemstein, A. P., van den Boom, H. J. J., and van Dijk, A. W., 1986, "Simulation of offshore heavy lift operations," in *CADMO'86: Proceedings of the International Conference on Computer Aided Design,, Manufacture, and Operation in the Marine and Offshore Industries* Washington, DC.

Yoon, J. S., Park, B. S., Lee, J. S., and Park, H. S. (1995) "Various Control Schemes for Implementation of the Anti-Swing Crane." *Proceedings of the ANS 6th Topical Meeting on Robotics and Remote Systems,* Monterey, CA, 472-479.

Zinober, A. S. I. and Fuller, A. T. (1973) "The Sensitivity of Nominally Time-Optimal

Control of Systems to Parameter Variation," *International Journal of Control*, 17:673–703.

Vita

Nader Ali Nayfeh was born on March 21, 1979 in Blacksburg, Virginia in the United States. He joined the Bradley Department of Electrical Engineering at Virginia Polytechnic Institute and State University in Blacksburg, Virginia in 1997. He received his Bachelor of Science in May 2001. Then, he immediately enrolled in the Master's of Science program at Virginia Tech.